
This is an electronic reprint of the original article.
This reprint may differ from the original in pagination and typographic detail.

Saani Shakil, Saani; Lu, Wei; Puttonen, Jari

Behaviour of vertically loaded steel beams under a travelling fire

Published in:
Structures

DOI:
[10.1016/j.istruc.2022.07.084](https://doi.org/10.1016/j.istruc.2022.07.084)

Published: 01/10/2022

Document Version
Publisher's PDF, also known as Version of record

Published under the following license:
CC BY-NC-ND

Please cite the original version:
Saani Shakil, S., Lu, W., & Puttonen, J. (2022). Behaviour of vertically loaded steel beams under a travelling fire. *Structures*, 44, 1-17. <https://doi.org/10.1016/j.istruc.2022.07.084>

This material is protected by copyright and other intellectual property rights, and duplication or sale of all or part of any of the repository collections is not permitted, except that material may be duplicated by you for your research use or educational purposes in electronic or print form. You must obtain permission for any other use. Electronic or print copies may not be offered, whether for sale or otherwise to anyone who is not an authorised user.



Behaviour of vertically loaded steel beams under a travelling fire

Saani Shakil^{*}, Wei Lu, Jari Puttonen

Aalto University, Department of Civil Engineering, Finland

ARTICLE INFO

Keywords:

Fire safety design
Travelling fire
Mechanical properties at elevated temperature
Heating and cooling stages in fire

ABSTRACT

As the structural response to a time and space dependent non-uniform temperature field is challenging to manage by code-based design, the behaviour of steel beams exposed to a travelling fire was simulated numerically in this paper. The finite element (FE) models for both thermal and mechanical analyses were validated by two benchmark tests and used to study the effect of uniform and non-uniform thermal exposures and different steel grades on the response of steel beams. The developed five-stage mechanism well characterized the response of the beams exposed to the travelling fire. For the beam in the elastic range, the heating-cooling cycles of gas temperatures induced cyclic axial forces, but the cyclic nature of structural responses was cushioned by material plasticity. For the beams stressed into the plastic range, the repetitions of cycles in axial response created residual deformations that induced catenary action in the beams at lower temperatures. The local heating of the critical sections made the beams more prone to a runaway failure than the uniform heating of the whole beam. Compared to the mild steel beams, the axial force response of the HSS beams showed higher axial compression forces and fluctuated more. The critical temperatures based on the deformation or strength criterion were consistent for the beams with the load ratio of 0.3. However, for designing the beam with the load ratio of 0.5, critical temperature of 350 °C or the strength criteria based on the proportional limit are recommended as the catenary action was activated at low temperatures. These recommendations can be used as a guide for practical design.

1. Introduction

Sustainable design solutions of steel framed buildings can be realized by using long-span beams with open, column-free spaces to advance building adaptability for future changes and by using high strength steel (HSS) to increase the strength-to-weight ratio. In open-plan compartments, fire can stay in one region and be modelled as ‘localised fire’ [1]. The fire can also burn locally and move across the floor, creating a non-uniform temperature field inside the compartment. The fire in this latter case is referred to as ‘travelling fire’ [2]. When an open-plan, steel-framed building is exposed to these fires, prescriptive structural fire design is often impractical and may lead to insufficient or superfluous structural fire protection [3] because of non-uniform thermal exposures and longer fire durations. As an alternative, performance-based structural fire design by using advanced analysis models is a reliable and cost-effective approach [4]. The non-uniform temperature fields arising from these types of fires can be computationally demanding for structural analysis and design, which encourages to develop the methods for evaluating the response of the structures to fire.

Research on the structural performance of the buildings exposed to travelling fires is topical. Dai et al. presented literature reviews [5,6] on experimental tests performed on buildings, analytical models developed for travelling fire, and case studies using travelling fire frameworks. The review pointed out the complexity of travelling fires and the needs of understanding of the physical mechanisms behind the fire scenarios and performing more travelling fire tests with refined simulations. Alam et al. performed two large scale fire tests for studying the effects of ventilation conditions on the development of surrounding steel members [7]. Their studies showed that significant non-uniform temperature fields developed not only along the length and width, but also along the height of the compartment. The highly non-uniform temperatures fields were also recorded both over the cross-sections and along the span of the steel beams. The travelling fire models were developed by Clifton [8] and Rein et al. [9,10], and were further extended to a framework of the travelling fire method by Dai et al. [5]. The travelling fire models have been applied to study the structural responses of different framed buildings exposed to horizontal and vertical travelling fires [11,12,5]. The studies revealed that the temperatures of structural members can be

^{*} Corresponding author.

E-mail addresses: saani.shakil@aalto.fi (S. Shakil), wei.2.lu@aalto.fi (W. Lu), jari.puttonen@aalto.fi (J. Puttonen).

<https://doi.org/10.1016/j.istruc.2022.07.084>

Received 14 March 2022; Received in revised form 8 July 2022; Accepted 28 July 2022

Available online 5 August 2022

2352-0124/© 2022 The Author(s). Published by Elsevier Ltd on behalf of Institution of Structural Engineers. This is an open access article under the CC BY-NC-ND license (<http://creativecommons.org/licenses/by-nc-nd/4.0/>).

higher when exposed to travelling fire scenarios than when exposed to the uniform (standard and parametric) fire. The study in [12] showed that the frames experienced irregular fluctuations of the axial forces and bending moments when the frames were exposed to the small travelling fire which moved from one bay to another bay. The oscillations of the structural responses were attributed to different bays being cooled at different times. On the other hand, Rackauskaite et al. reported no significant cyclic movements of columns inside steel framed buildings exposed to vertically travelling fire as observed in other types of frames [11,12]. They concluded that these differences could be due to a different structural system or small number of fire floors. In all these studies, the fire curves produced by the travelling fire models were smooth curves including one peak. However, Ramsamy et al. reported the double peaks of adiabatic surface temperatures at ceilings for different ventilation conditions [13]. According to them, the second peak has not been predicted by the travelling fire methodology. Besides the double peaks, the temperature–time profiles also had multiple local peaks. The effect of the local heating–cooling cycles of the temperature–time profiles on the structural responses have not been studied thoroughly. Therefore, the mechanisms for inducing the cyclic structural responses of the members and how these cyclic responses affect structural fire design of the members require more investigations.

Design code such as EN 1993-1-2 [14] assesses the fire resistance of beams inside the framed structures based on the performance of isolated members in standard furnace tests [15–17]. The failure of the member is defined according to either the deflection criteria as given in [18,19] or the load levels at which the beam loses its load-carrying capacity [14]. The beams with high axial restraints can endure high temperatures without runaway failure by activating catenary actions. High axial restraints can lower the beam deflection, thus protecting the integrity of the structure [20–24]. A non-uniform temperature field over the cross-section due to the low thermal conductivity of the concrete slab supported by the beam is often considered in design. Along the span, a uniform temperature field is often assumed. According to [25,26], the non-uniform temperature distribution along the beam arisen by a localised fire can be more detrimental and can change the nature of the structural response compared to beam behaviour under uniform temperature field. The travelling fire, which is a localized fire that moves, can have an even more adverse effect. The studies in [11] showed that the steel frames with 1–3 floors had material strength failure at temperatures between 600 °C and 700 °C, whereas the frames with over 5 floors failed by thermal expansions and geometric effects at temperatures as low as 130 °C. In addition, the studies in [27] showed that the mechanical properties of HSS at elevated temperatures differ from those of mild steel. The response of the HSS beam due to non-uniform temperature distribution can be different from the response of mild steel beams. Therefore, further research is necessary to investigate the applicability of the criteria of defining the failure of both mild steel and HSS beams exposed to non-uniform temperature fields along the span.

The purpose of this research is to study the effects of travelling fires on the load-bearing mechanism of beam structures, evaluate the applicability of the available failure criteria for the beams exposed to travelling fires, and determine the critical temperatures that can further be applied to the practical design. The research is organized as follows: The finite element (FE) models for thermal analyses are developed considering the effect of non-uniform temperature distribution both over the cross-section and along the beam span. The FE mechanical analysis which considers both geometric and material non-linearity is used to evaluate the deformation behaviour of the beams. The models are validated and verified by benchmark test results. The validated models are used to study the load-bearing mechanism of beams with the following parameters: fire scenario, span length, load ratio, and steel grade. Based on the load-bearing mechanism, the critical temperatures of the studied beams are proposed by using different criteria.

2. FE modelling and validation

2.1. FE models for steel beams tested inside furnaces

2.1.1. FE models for a 4.5 m steel beam

The FE models are based on the benchmark test of a 4.5 m long steel beam conducted in 2007 [16]. This beam has been used in several studies [22–24,28] for the validations of FE models. The beam was simply supported and had a profile of H250 (250 × 250 × 8 × 12 mm). The top flange was protected by a 3 mm thick ceramic fibre blanket to simulate the thermal effects of a concrete slab. The steel grade of the beam was Q235B, with a measured yield strength of 271 N/mm². Two concentrated loads of 130 kN were applied symmetrically at 750 mm from the centre of the beam at room temperature. The loading was maintained throughout the test. During the tests, the beam was subjected to the heating and cooling. The beam was kept inside the furnace after the heating was turned off at 19 min. The furnace had a maximum temperature of 844 °C in the tests. The test was terminated at 148 min from the start of heating.

The FE models for both thermal and mechanical analysis were created similar to the models in [23]. The thermal analysis was performed using Abaqus/Standard [29], and the mechanical analysis was performed using Abaqus/Explicit [29]. Fig. 1(a) presents the two-dimensional FE model created for the transient thermal analysis. The beam section including the ceramic fibre was discretised with 2128 linear heat transfer elements (DC2D4). The nonuniform temperature across the cross section was considered by using different thermal properties for steel and the ceramic fibre protection. According to [30], the density of ceramic fibre was taken as 128 kg/m³, and the temperature dependent thermal conductivity of the ceramic fibre was varied from 0.06 W/m.K at 260 °C to 0.3 W/m.K at 1093 °C. The thermal properties of the steel were adopted from EN 1991-1-2 [31]. The convection coefficients used for the steel and the ceramic fibre blanket were 25 W/m²K and 9 W/m²K, respectively. The resultant emissivity of 0.7 was used for the steel beam and 0.5 was used for the ceramic fibre blanket. The values of emissivity and convection coefficients in the figure have been used previously for the exposed and unexposed surfaces in literature [22,26,31,32]. The interaction between top flange and ceramic fibre was modelled with a large value of gap conductance and a zero gap for lossless thermal conduction. The beam was heated and cooled according to furnace temperature curve shown in Fig. 2. The temperature field output from thermal analysis was used as a thermal boundary condition in the mechanical analysis. The three-dimensional FE model with boundary conditions for mechanical analysis and a part of the mesh discretisation of the beam are shown in Fig. 1(b) and (c), respectively. In total, 9640 linear quadrilateral shell (S4R) elements were used to mesh the whole beam. The stress–strain curves and the temperature-dependent reduction factors used for the steel were as defined in EN 1993-1-2 [14].

2.1.2. Validation of FE models of a 4.5 m beam

The FE model for thermal analyses was validated by comparing the temperature development of the bottom flange and the top flange of the beam between the FE simulation and the test [16] in Fig. 2. The comparison showed that the temperatures calculated for the bottom and the top flanges of the steel beam were close to the test values in the heating stage but were lower than the test values in the cooling stage. In general, the FE and test results matched well. In addition, for the bottom flange, the combination of higher values of the emissivity and convection coefficients gave a better match for the test results in the heating phase, while the combination of the lower values gave a better match in the cooling stage. For the fire-protected top flange, the combination of the lower values led to a better match with the test results. Based on this comparison, the values of the emissivity and convection coefficients of the bottom and top flanges, as presented in Fig. 1(a) were selected for further studies.

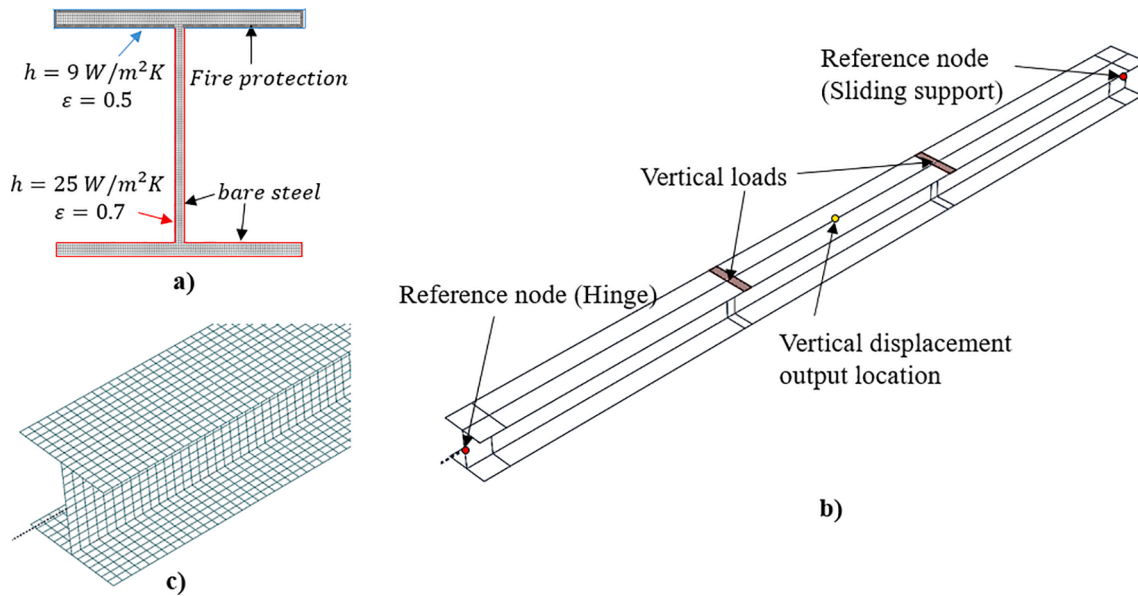


Fig. 1. FE models for thermal and mechanical analysis: (a) The 2D FE model with mesh and boundary conditions for thermal analysis (b) Restrained steel beam with loads and boundary conditions for mechanical analysis [23] (c) Mesh discretisation of the beam model for mechanical analysis.

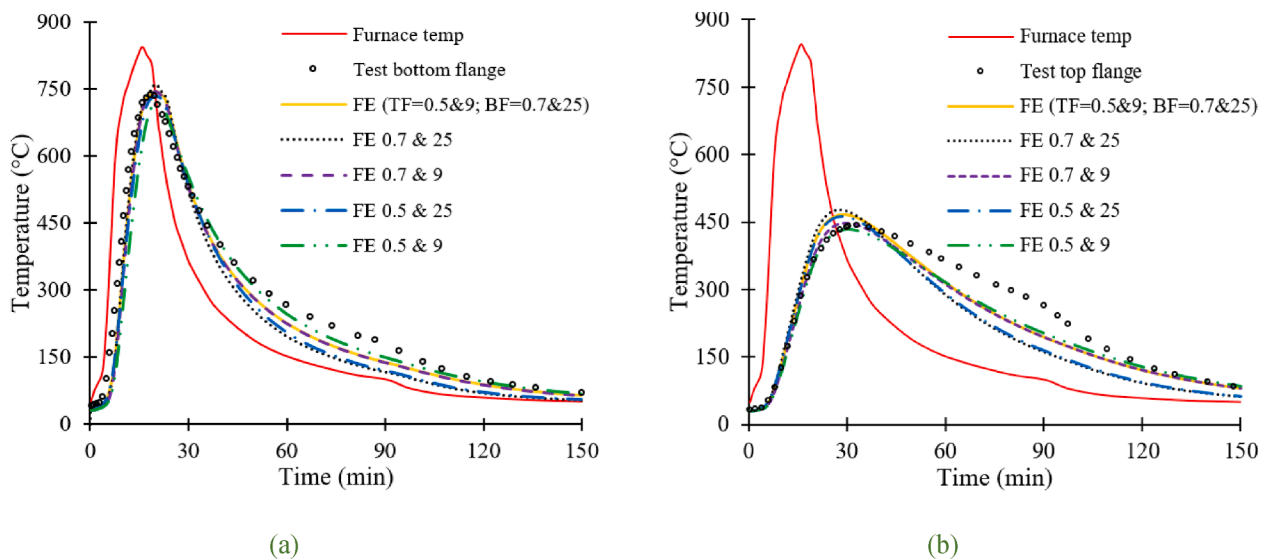


Fig. 2. Temperature development of the steel beam using different values of emissivity (0.7 and 0.5) and heat transfer coefficient (25 and 9 W/m²K) in the (a) bottom flange (BF) and the (b) top flange (TF).

The FE model for mechanical analyses was validated by comparing the deformation mode and the mid-span displacement of the beam between FE analyses and the test in Fig. 3(a) and (b), respectively. As indicated in Fig. 3(a), the bottom flange buckling observed in the test [16] was captured in the FE simulation. Fig. 3(b) shows that the mid-span displacements received from the FE analysis coincide with the test values [16]. The reasonable agreement between FE and test results also indicated that the exclusions of initial geometrical imperfections and residuals stresses in the mechanical model have minor effects on the beam responses. The observations have been pointed out in [23].

2.1.3. Validation of FE models of a 2 m beam

In addition to the validation by the 4.5 m beam, the FE models were further validated by a 2 m beam tested inside a furnace by Liu et al. [17] in 2002. The beam had 178 × 102 × 19UB (S275) section with 15 mm thick ceramic fibre protection on the top flange. The beam in the test was

heated by the furnace fire which followed the ISO834 standard fire curve. The furnace was then turned off at 41 mins and the beam was kept inside thereafter. The temperature development of the beam is compared between the FE simulation and the test [17] in Fig. 4. The temperatures of the top flange and the bottom flange of the beam obtained from thermal analysis matched well with the measured values of the test. The time dependent temperature distribution of the 2 m beam obtained from the thermal analysis was used as input data in the mechanical analysis.

The FE model of the 2 m beam for mechanical analyses has similar meshes and boundary conditions as the 4.5 m beam shown in Fig. 1 except that the 2 m beam had axial restraint of 8 kN/mm. At room temperature, two vertical loads of 40 kN were applied symmetrically at 400 mm from the mid-span and maintained during the heating and cooling stages. The FE model of the 2 m beam was validated by comparing the mid-span displacement and the axial compression force

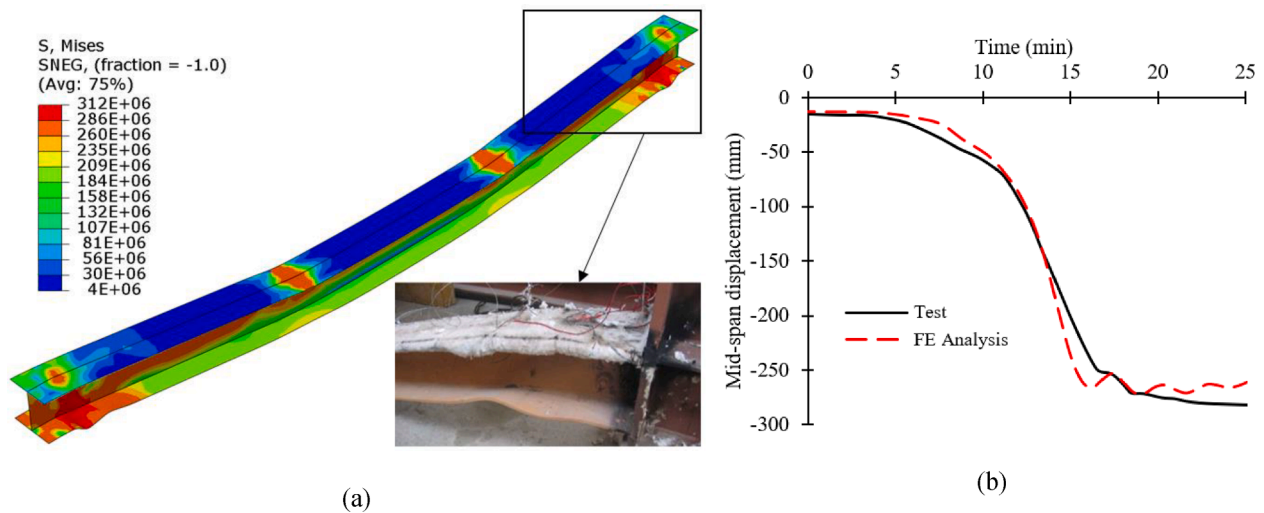


Fig. 3. Comparison of FE analysis of the beam with test results: (a) Deformation mode (stress units in N/m^2), (b) Mid-span displacement.

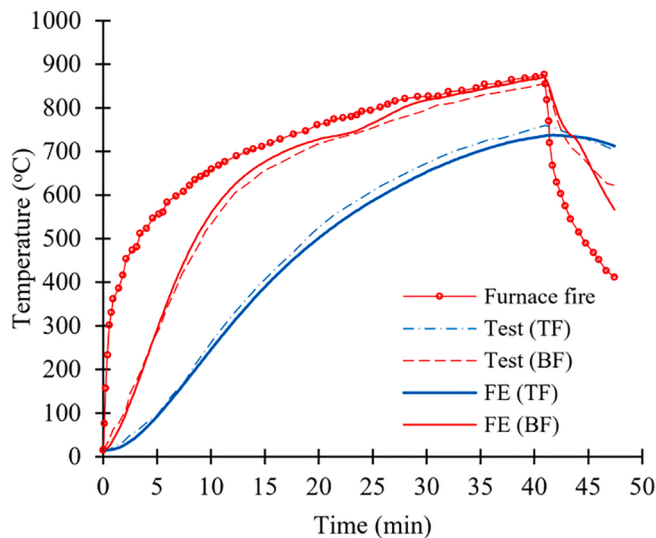


Fig. 4. Temperature development of the steel beam in the FE analysis compared to the temperatures measured in the test for the (a) bottom flange (BF) and the (b) top flange (TF).

between the FE analyses and the test results [17] as shown in Fig. 5. Fig. 5(a) shows that the FE analysis slightly underpredicted the initial displacement, but the overall FE values matched well with the test values. Fig. 5(b) shows that the axial force matched well between the FE analysis and the test and reached similar peak before the sudden drop caused by accelerated mid-span deflection of the beam. The FE analyses predicted the same critical temperature of the beam as in the test.

In summary, for both 4.5 m and 2 m beams, the FE analysis results agreed well with the test results. Similar modelling methods have also been used for the validation of FE models in [33]. Therefore, the validated FE models are suitable for thermal and mechanical analyses of steel beams exposed to the heating and cooling stages of fire.

2.2. FE models for 9 m steel beam exposed to non-uniform temperatures along the span

2.2.1. FE thermal analyses models in 2-D and 3-D domain

A three-dimensional FE model capable of resolving temperature non-uniformity over the section and along the span was developed. This beam model is based on a 9 m long beam tested inside a building

exposed to a travelling fire [34]. Fig. 6(a) illustrates the section view of the building and the location of the beam. The steel beam with a profile of IPE 270 had a concrete slab on top without additional loading. In the test, the fire originated from the left side of the beam and travelled along the span towards the right.

Fig. 6(b) illustrates the global view of FE model of the studied beam non-uniformly heated by the gas temperatures (TG1, TG2, and TG3). The gas temperatures provided in [34] were applied at three different locations along the beam to represent the travelling fire in the simulation. Compared to the furnace fire (Fig. 2), the fire inside the studied building (Fig. 6(c)) had the following three features:

- (i) For the whole period, the fire curves at different locations behaved like a slowly developing fire, i.e., they had a similar growth rate at the beginning, different rates of rise before peaks and similar rates of decay after the burnout of the fuel.
- (ii) The fire curves reached their peak values at different times and at different locations.
- (iii) Along the travelling path, the peak of the fire curve at the burning region resulted in the heating-cooling cycles of the fire curve at the burned-out region or changed the heating rate of the fire curve in neighbouring region.

The heating and cooling phases of the travelling fire are described by the points shown in Fig. 6(c) as follows:

- Point 0 to 1: the rise of the gas temperature close to the beam due to the burning of the fuel in TG1 region.
- Point 1 to 2: the rise of the gas temperature close to the beam due to the travelling of the fire from TG1 region to TG3 region.
- Point 2 to 3: the decrease of the gas temperature close to the beam from the corresponding maximum values in TG1, TG2, and TG3 region due to the cooling of the fire in TG3 region.
- Point 3 to 4: uniform distribution of the gas temperature over the span during the cooling phase.

The effects of these features of the fire curves on the beam response were studied further.

Since thermal conduction along the span is important for the beam exposed to non-uniform temperatures, the beam was modelled in 3-D domain. The non-uniform temperature across the cross section was considered in thermal analysis by using the concrete slab with thermal properties adopted from [34] with specific heat of 1.04 kJ/kg.K and thermal conductivity 1.4 W/m.K . Temperature development of the steel

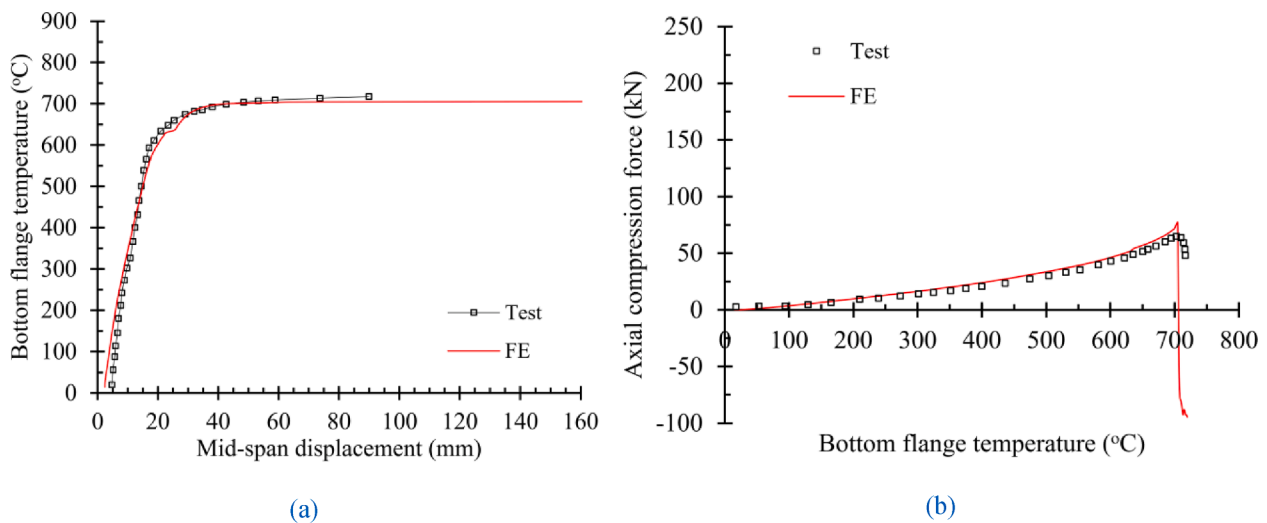


Fig. 5. Comparison of FE analysis results with test results for the 2 m beam: (a) Mid-span displacement (b) Axial compression force.

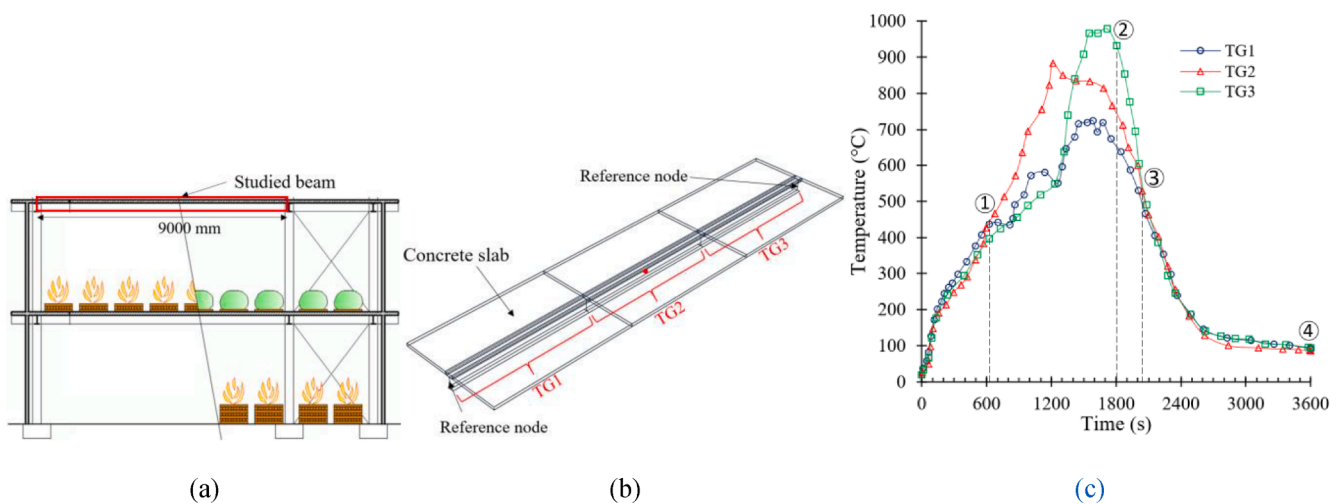


Fig. 6. A 9 m long beam selected from a building test for FE modelling (a) Vertical section of the test [34] (b) FE model of the beam (c) Temperature curves of TG1 to TG3 (TG: Gas temperature).

beam was not presented in the 9 m beam test [34], therefore, the FE model in 3-D domain (hereafter, 'FE 3Dt') was first verified in section 2.3.2 using the temperature values received by the validated FE model in 2-D domain (hereafter, 'FE 2Dt'). The models and the corresponding boundary conditions are shown in Fig. 7. In the FE 2Dt model (Fig. 7(a)), the steel beam and concrete slab were discretised using DC2D4 elements, which are 4-node linear heat transfer quadrilateral elements in Abaqus [29]. Only a portion of the 60 mm thick concrete slab is shown in the figure. Convection and radiation boundary conditions were applied to the exposed and unexposed surfaces in the model, and the values of the emissivity and convection coefficients were defined according to the recommendation for advanced fire models in EN 1991-1-2 [31]. In the FE 3Dt model (Fig. 7(b)), the steel beam was discretised using shell elements (DS4), while the concrete slab was discretised using solid heat transfer elements (DC3D8). The same thermal boundary conditions defined for the FE 2Dt model were adopted, but they were extended into the third dimension for the FE 3Dt model.

2.2.2. Verification of FE 3Dt model using the validated FE 2Dt model

In Fig. 8, the temperature development of the cross-section at the mid-span of the beam using the FE 3Dt and FE 2Dt models are compared. The beams were uniformly heated using the TG1 fire curve. The figure

proves a good agreement between the temperatures received using the two models. A similar agreement of temperature was observed when the beam was heated using the TG2 and TG3 curves. The temperatures obtained using the FE 3Dt and FE 2Dt models indicate that both models have similar accuracy. Since the FE 3Dt model includes thermal conductivity along the span and can produce the nodal temperatures needed as boundary conditions in the FE models for mechanical analyses, this model was used for parametric studies.

In the test, the beam was heated non-uniformly using the TG1, TG2 and TG3 temperature curves simultaneously at different parts along the span as depicted in Fig. 6(b). The FE 3Dt model was further verified using the simulation results which were calculated with the FDS solver (Fire Dynamics Simulator) [35], as given in [34]. Fig. 9 shows that the time-temperature curves generated by the FE and FDS analyses have similar trends but different values. The solver in FDS is one-dimensional and is unable to capture the heat conduction mechanism accurately inside the beam. In addition, a limitation arises due to mesh discretisation in FDS, since the software is primarily intended for solving computational fluid dynamics (CFD) problems. For the studied beam, it is reasonable to assume that FE analysis gave more accurate temperatures than FDS analysis. The FE models verified for thermal analyses in this section were coupled with FE models for mechanical analyses for

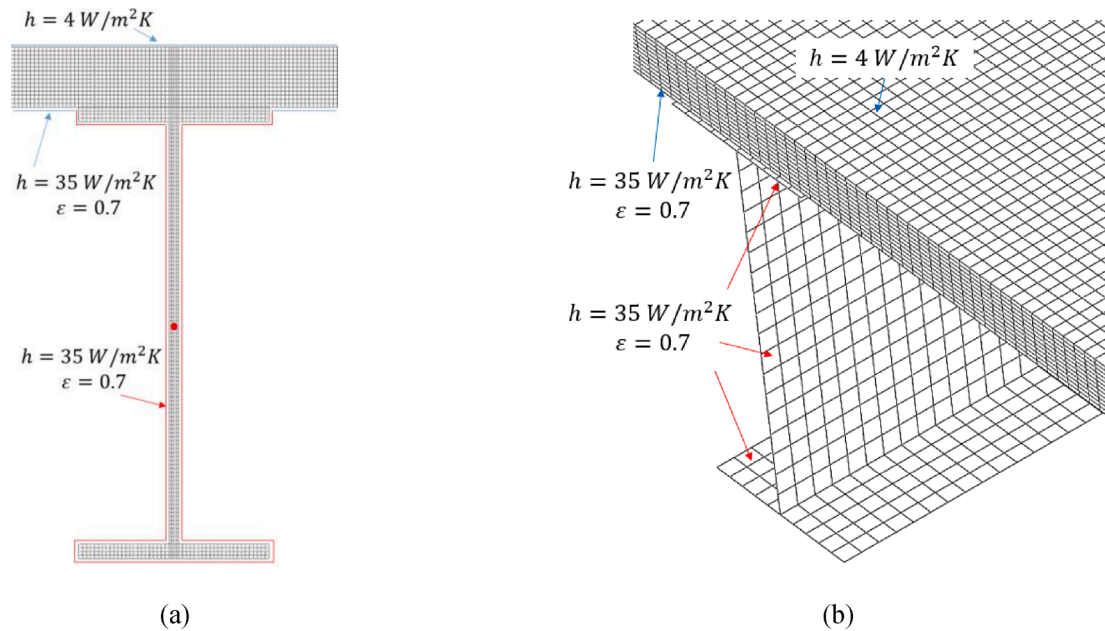


Fig. 7. Mesh discretisation and thermal boundary conditions for (a) the FE 2Dt model and (b) the FE 3Dt model.

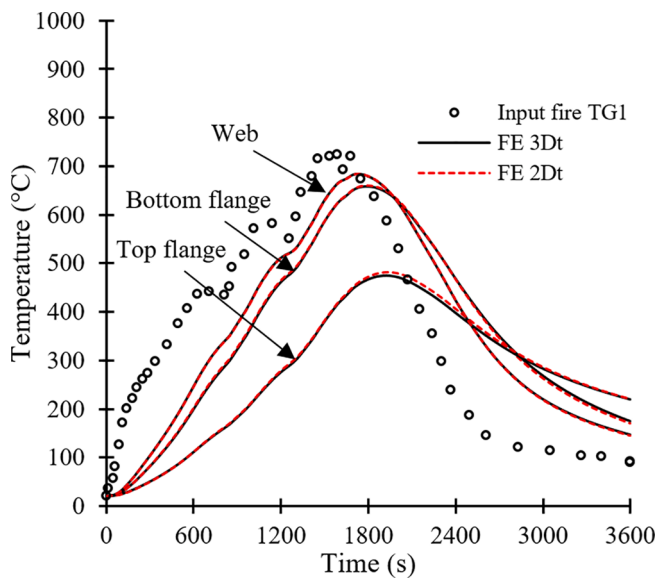


Fig. 8. Comparison of temperature development at mid-span of the beam between FE 2Dt and FE 3Dt models using TG1 fire curve as input.

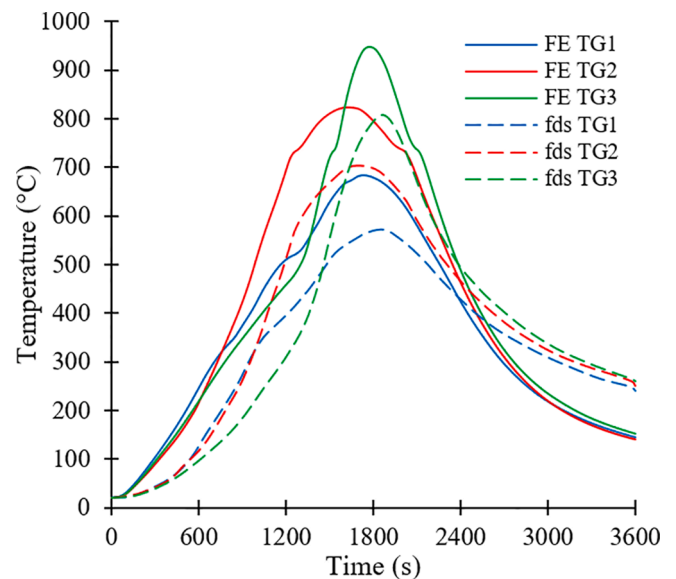


Fig. 9. Steel temperatures of the web from FE 3Dt model compared with the FDS results [34] recorded at the middle of the beam segments heated by TG1 to TG3 fire curves.

studying the beam responses.

3. Load-bearing mechanisms of steel beams exposed to different temperature fields

The validated and verified FE models were used to study the effect of fire exposures also including the travelling fire on the load-bearing mechanism of steel beams. Table 1 summarizes the studied spans and the fire exposures of the steel beams. In the studies, short and long beams were represented by span lengths of 4.5 m and 9 m, respectively. The 4.5 m steel beam was respectively heated uniformly along the span using the furnace fire curve presented in Fig. 2 and the TG1 curve presented in Fig. 6(c). The 9 m long beam was uniformly heated along the span using the TG1, TG2 or TG3 curve presented in Fig. 6(c). Non-uniform temperature distribution along the span was created by the

Table 1

Span lengths, support conditions and types of fire exposure of the studied beams.

Span (m)	Support condition	Fire exposure
4.5	Pinned-pinned	Furnace fire, TG1
9	Fixed-fixed	TG1, TG2, TG3, Travelling fire

simultaneous use of the TG1 to TG3 curves along the span as depicted in Fig. 6(b) (hereafter, also referred as ‘travelling fire’). All the steel beams had a profile of IPE 450 and a nominal yield strength of 355 N/m². A 60 mm thick concrete slab on the top of the steel beam was included in the thermal analyses to introduce non-uniform temperature field about the cross-section but the slab was excluded from the mechanical analyses. However, in the mechanical analyses, the stiffening effect of the

concrete slab on the behaviour of the steel beam was included by restraining both the lateral displacement and torsional twist of the top flange. The thermal boundary conditions of the beams were defined similarly as described in Section 2.3.1. In the mechanical analysis, the 4.5 m beam had pinned supports. As indicated by the studies in [36], the beams with full axial restraints behaved similarly to the beams with axial restraints equal to the beam stiffness, and the behaviour of the beams with slight axial restraints resembled more to the behaviour of the beam with full axial restraints. Therefore, full axial restraints were used for the 9 m beam at its two ends. The axial restraints were also necessary to satisfy the deflection criteria at room temperature. The beams were loaded uniformly with a load ratio of 0.3. Load ratio was defined as the ratio of the maximum bending moment due to the applied load to the plastic bending capacity of the beam structure at room temperature [37].

3.1. Response and load bearing mechanism of the 4.5 m long beam heated by furnace or TG1 fire curve

3.1.1. Responses of the studied beams

The responses of the 4.5 m beam exposed to the furnace fire and the TG1 fire are reported in this section. Fig. 10 and Fig. 11 present the FE results for the temperature development at the mid-span and the axial force resultants in the main parts of the end section due to the furnace fire, mid span displacement and axial force response due to both the furnace fire and TG1. As the bending moment at end supports is close to zero, the section forces mainly indicate the variation of the temperature-induced axial forces.

Fig. 10(a) shows that the peak of temperatures of the top flange of the beam were significantly different from those of the web and the bottom flange due to the heat sink effect of the concrete slab. The consequence of the non-uniform temperature field was that the temperature-induced degradation of the material properties happened at different times in different parts of the cross-section, thereby affecting the development of mid-span deflection and the axial force response. As indicated by the section forces in Fig. 10(b), before point 3 and after point 6, thermally induced compressive and tensile forces inside the beam were mainly controlled by the web temperatures because the forces of the web were greater than those of the flanges. However, between point 4 and point 8, the beam response was controlled by the non-uniform temperature field over the whole cross-section. As shown in Fig. 11(a), the beam deflected at a different rate upon heating and gradually recovered at a different

rate during the cooling phase. Similarly, the thermally induced forces changed from compression to tension at a different rate as shown in Fig. 10(b) and Fig. 11(b).

Compared to the furnace fire curve, the TG1 curve reached a lower maximum temperature with a slower heating rate, included local heating-cooling cycles, and had a longer duration. The FE results for the mid-span displacement in Fig. 11(a) showed that the characteristics of the TG1 curve decreased the beam deflection during the heating stage and increased its recovery during the cooling stage compared to the effects of the furnace fire. The FE results for axial forces in Fig. 11(b) showed that the beam heated by TG1 curve compared to the beam heated by the furnace fire had larger axial force at the beginning of fire as the lower level of temperatures inside the beam prolonged its elastic range. This larger axial force entered both the web and the bottom flange in a non-linear range initiating the local buckling of the web before 400 °C, which led to a sudden change in the axial force. As the temperature field in the beam developed at a slower rate and included local heating-cooling cycles, the material properties degraded more slowly. This delayed the transition from compression to tension in the beam leading to a higher axial tension force during the cooling stage. In addition, the local heating-cooling cycles of the TG1 curve induced more fluctuations of the axial force response in the beam.

3.1.2. Load-bearing mechanism of the studied beams

According to the temperature-induced force responses and the degradation of the material properties, the load-bearing mechanism of the studied beams can be divided into five stages:

1. Stage 1 (points 0–1) was characterized by the activation of the axial compression. The axial compression force was developed due to the restrained thermal expansion. The magnitude of the compression force depended on the axial stiffness of the beam, the stiffness of the support and the temperature distribution inside the beam. The stage ended when the material properties started to degrade.
2. Stage 2 (points 1–5) was characterized by the decrease of the axial force response due to the degradation of mechanical properties, the yield of the material and the instability or formation of the plastic hinge mechanism of the beams. The degradation of the elastic modulus retarded the increase in the axial force in compression and enlarged the deflection of the beam. The degradation of the yield strength promoted the yielding inside the beam and further decreased the compression force developed axially. The next stage

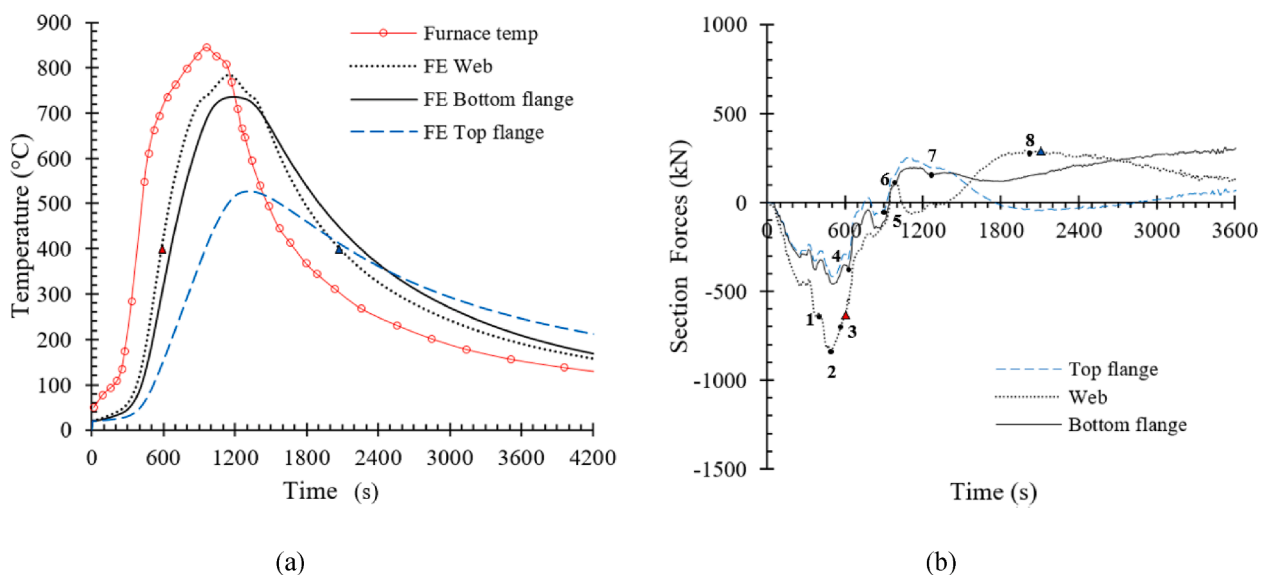


Fig. 10. Response of the 4.5 m steel beam with a concrete slab on top exposed to furnace fire: (a) Temperature development (b) Section force at end-support.

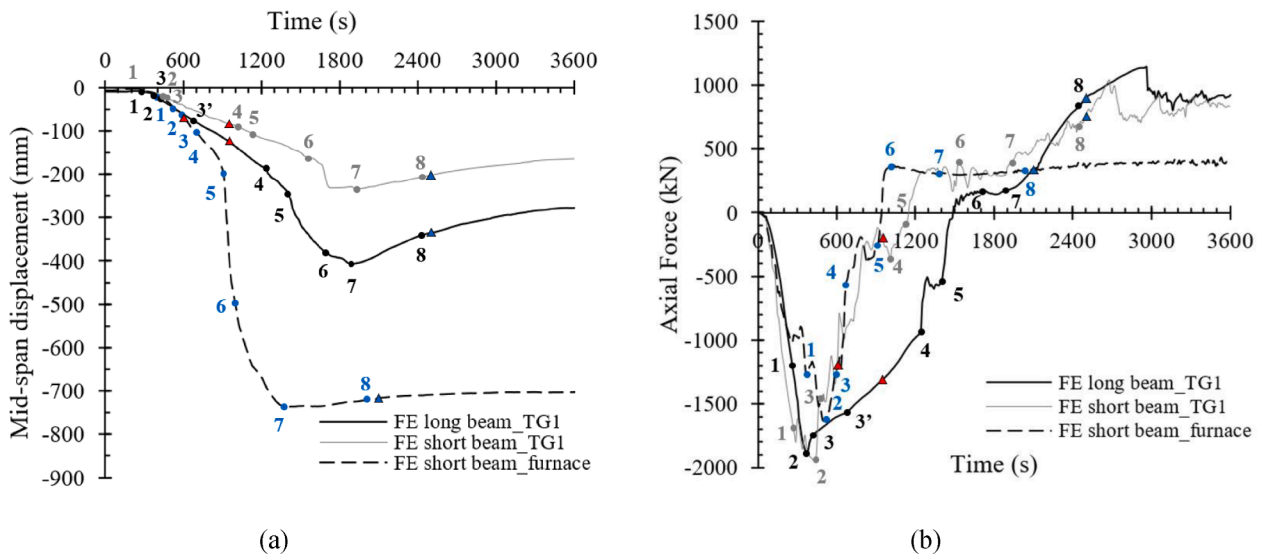


Fig. 11. Response of the 4.5 m beam exposed to furnace fire and TG1 curve and the 9 m beam exposed to TG1 curve: (a) Mid-span displacement (b) Axial force response at end-support.

started when a large deformation occurred due to the hinge mechanisms or the instability of the beam.

- Stage 3 (points 5–6) was characterized by the transition of the axial force response from compression to tension due to large beam deformations that activated the catenary action. The cooling of the beam can also activate this transition. The end of this stage was indicated by the local peak of the axial tension force.
- Stage 4 (points 6–8) was characterized by the development of axial tension in all parts of the beam section. The decrease in the axial force at this stage was caused by the increased deformation of the beam caused by further heating or partly cooling down. The maximum displacement typically occurred during this stage, and the end of this stage was indicated by cooling of the beam back to 400 °C.
- Stage 5 (point 8 onwards) was characterized by the increase in axial tension force caused by restrained contraction of the cooling beam. The axial tension force was developed gradually if no material failure occurred in the beam.

3.2. Response and load bearing mechanism of the 9 m long beam heated with different fire curves

3.2.1. Response of the 9 m long beam heated uniformly with TG1, TG2, or TG3 curve

The response of the 9 m long beam heated with TG1 curve was firstly studied. The temperature of the cross-section at mid-span and the section forces at the end-support received from the FE simulations are shown in Fig. 12(a) and (b), respectively. The FE results of the mid-span displacement and the axial force response are added in Fig. 11(a) and (b), respectively.

Fig. 11 and Fig. 12(b) show that the 9 m long beam behaved similarly to the 4.5 m long beam but with some detailed differences. For the axial force in the 9 m beam, the curves in Fig. 11(b) indicate a gradual change towards point 4, a delayed transition between point 5 and point 6 and higher tension forces after point 7. The features of the axial force in the 9 m long beam were due to the formation of the hinges at fixed supports,

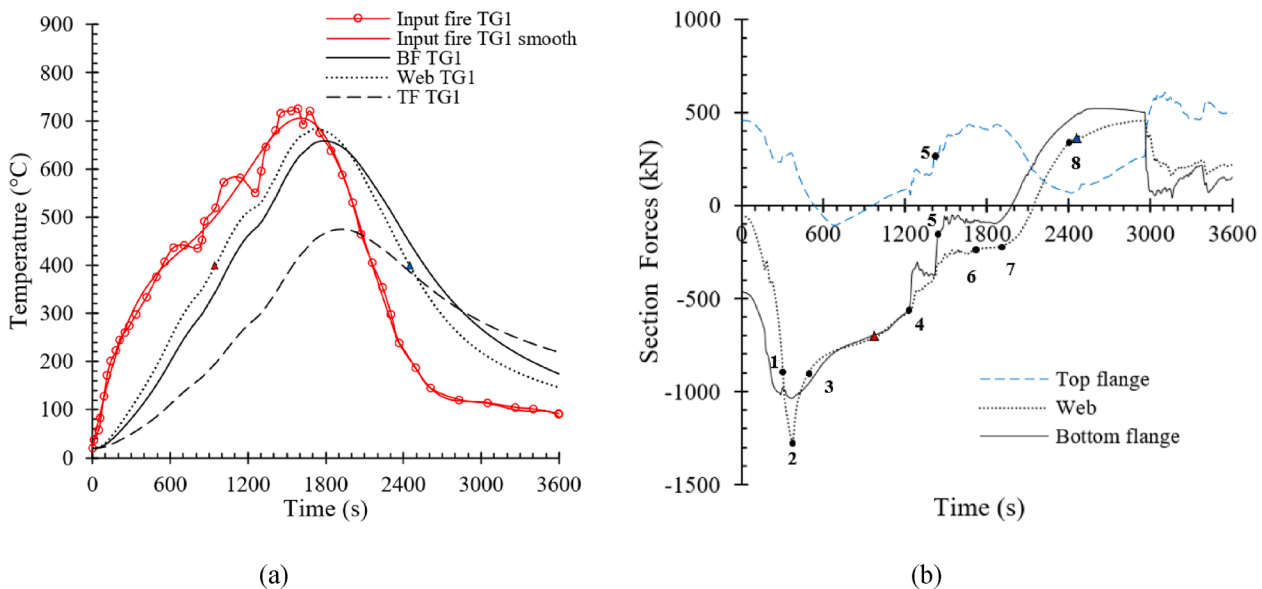


Fig. 12. Response of the bottom (BF), top flange (TF) and the web of a 9 m steel beam with a concrete slab on top exposed to TG1 curve: (a) Temperature development (b) Section force at end-support.

the lower axial stiffness, and the slow-developed fire. During the TG1 fire, these factors also delayed the accelerated mid-span displacement of the 9 m long beam as shown in Fig. 11(a) and (b). The curves for the section forces in Fig. 12(b) show that the fluctuations of the axial forces were observed more in the flanges than in the web.

The responses of the 9 m long beam heated with TG2 or TG3 curve are compared in Fig. 13 with that of the same beam heated with TG1. The points 1 to 4 in Fig. 13(b) correspond to the heating and cooling stages of the fire curves in Fig. 6(c). All the fire curves affected the responses of the beam similarly up to the point 3 because of the similar temperature fields and initial stress state inside the beam. From that point onwards, the beam behaved differently.

The beam heated by the TG2 curve started the transition from compression to tension at 1200 s, which is 200 s and 300 s earlier than in the beam heated by TG3 and TG1 curves, respectively. The heating-cooling cycles and the lower temperatures of the TG1 curve delayed the transition of the TG1-exposed beam. Compared to the temperatures of TG1 curve, the higher temperatures of TG3 curve accelerated the transition of TG3-exposed beam. However, compared to the maximum temperature of TG2 curve, the later reached maximum temperature of TG3 curve delayed the transition from compression to tension. In the end, the beam heated by the TG3 curve failed in a runaway deflection mode, whereas the beams heated by the TG1 and TG2 curves survived by hanging on the supports. The beams heated by TG1 and TG2 curves deflected less than the TG3-exposed beam, therefore, they developed larger axial tension force as they survived the whole cooling period. The maximum beam deflection due to the TG2 curve was larger than the maximum deflection due to the TG1 curve but close to the maximum deflection due to the TG3 curve. The cyclic axial force response observed in the beam heated by the TG1 curve was not observed in the beams heated by other curves. In general, the response of the beams was directly proportional to the magnitude of the temperatures, the rate of the temperature development and the non-uniform temperature field over the cross-section.

3.2.2. Response of the 9 m long beam exposed to travelling fire described by TG1 to TG3 curves

The fire curves TG1 to TG3 were applied along the beam according to the scheme in Fig. 6(b) and the temperatures were recorded at the web along the span are presented in Fig. 14. As shown in the figure, the temperatures at the transition region TG1-TG2 were in between the temperatures recorded at the middle of the segments of TG1 and TG2.

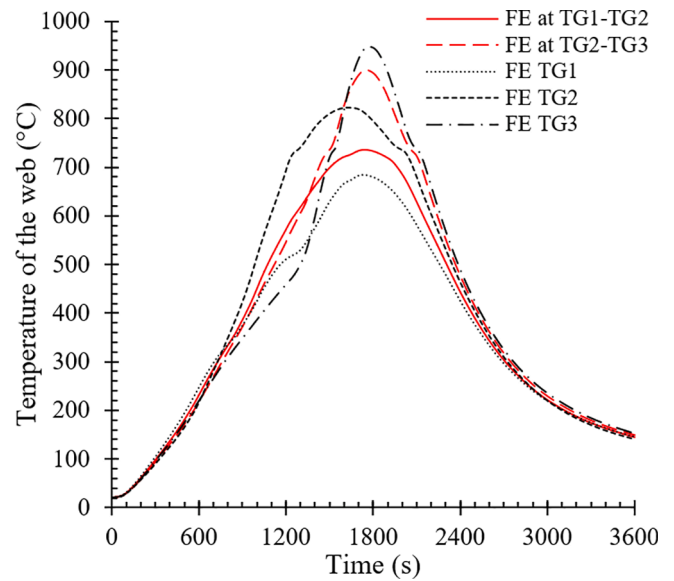


Fig. 14. Steel temperatures along the 9 m beam exposed to travelling fire with outputs taken from the centre of the web at the middle of TG1, TG2, and TG3 segments and at the transition regions TG1-TG2 and TG2-TG3.

Similarly, the temperatures at the transition region TG2-TG3 were in between the temperatures recorded at the middle of TG2 and TG3 segments. The non-uniform temperature field along the span was clearly observed between 800 s and 2400 s when the TG2 curve started to increase and the TG3 curve started to decrease.

The mechanical responses of the 9 m beam heated by the travelling fire are presented in Fig. 13(a) and (b). The behaviour of this 9 m beam was consistent with the five-stage mechanism but followed the non-uniform temperature field developed inside the beam. Under non-uniform heating conditions ('all temps' in the figure), the beam initially behaved according to the temperature field close to the location of fire ignition (FE TG1), developed the transition from compression to tension due to a large deflection caused by temperatures close to the location at the mid-span (FE TG2) and hanged from the support by a catenary action and later on experienced runaway deflection based on the temperatures close to the end of the travelling path (FE at TG2-TG3 and FE TG3). The large deformation of the beam occurred when the

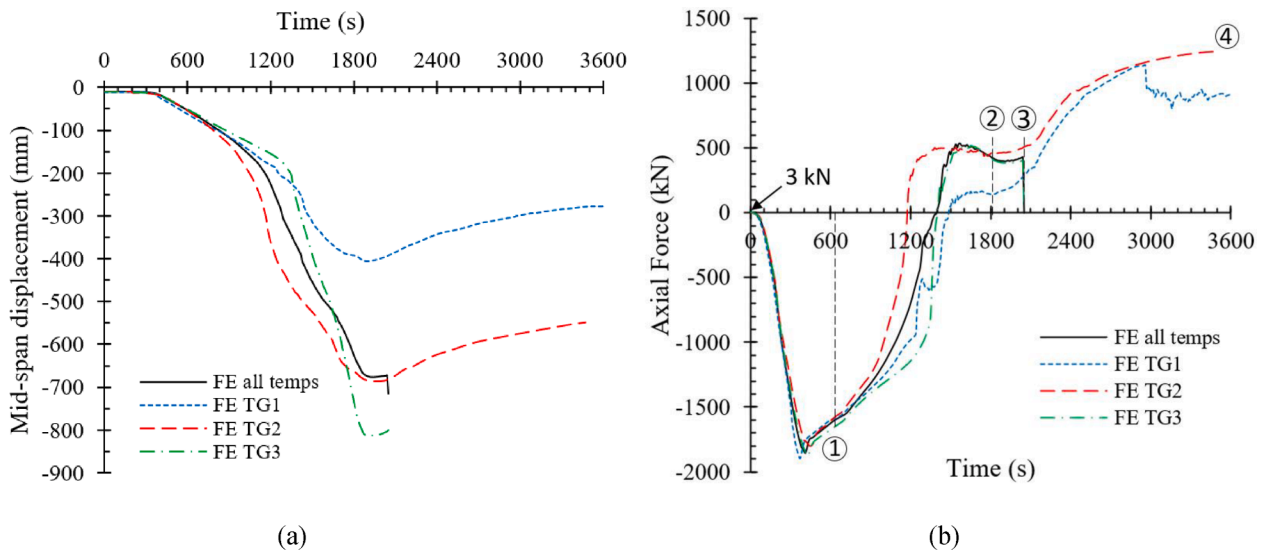


Fig. 13. Response of the 9 m long beam heated uniformly using TG1 to TG3 curves and simultaneously using TG1 to TG3 curves (all temps): (a) Mid-span displacement (b) Axial force response at end-support.

global hinge mechanism inside the beam was activated as the fire travelled. In addition, the fluctuations of the axial force were not observed because the behaviour of the beam in the later stage was affected more by the smoother TG2 and TG3 curves rather than the TG1 curve. These observations suggest that the occurrence of fluctuations in the axial force response depends on the profile of the gas temperatures especially between point 1 and point 3 shown in Fig. 13(b) when the beam was heated non-uniformly along the span.

4. Effect of different parameters on the Load-Bearing mechanism of the 9 M beam exposed to travelling fire

Using the five-stage load-bearing mechanism, the effects of different parameters on the load-bearing mechanism of the 9 m beam are investigated in this section. The studied parameters include the local heating-cooling cycles, the span of the beams, the heating locations, the load ratios, and the steel grades.

4.1. Effect of the local heating-cooling cycles on the response of 9 m long beam

The effects of the local heating-cooling cycles of the TG1 curve on the beam response were studied by intentionally smoothing the TG1 curve. The resulting curve is designated as 'TG1 smooth' and is presented in Fig. 12(a). The figure shows that, in the region where TG1 curve has local cycles, the TG1 smooth curve has a clear increase in the heating rate.

When exposed to the TG1 or the 'TG1 smooth' curve, the beams deflected with the same trend, but had slightly different magnitudes as shown in Fig. 15(a). For the axial force response, the curves in Fig. 15(b) have similar trends but with more observable differences after point 2. The beam heated by the smooth curve developed a slightly higher axial compression force at point 2, took a slightly longer time to reach point 4, moved to point 5 more smoothly, had a quicker transition from point 5 to point 6 and developed a higher axial tension force during the cooling stage.

The different axial forces in two beams between point 4 and point 5 are explained by the stress contour shown in Fig. 16. At 1300 s, the two beams had similar stress contours in the web and the flanges. However, compared to the beam exposed to the 'TG1 smooth' curve, the beam exposed to TG1 curve yielded less in the top flange and had lower stresses in the web close to mid-span. The TG1-exposed beam had more elastic regions, leading to the fluctuations of the axial forces when it

experienced heating-cooling cycles. This observation suggests that the beam in the elastic range is more sensitive to the fluctuations induced by the thermal cycles. In addition, simplifying the fire curve by smoothing can lead to a similar mid-span displacement but smoother local stress cycles.

4.2. Effect of the span length on the response of the beams

The effects of the span length and the mechanical boundary conditions were studied by comparing the responses of both the 4.5 m and 9 m long steel beams exposed to the TG1 fire. As shown in Fig. 11, the two beams have the similar trend of the axial forces due to similar load-bearing mechanism but have observable differences between the points 3 and 8. In the 9 m beam, the fluctuations of axial forces between the points 3 and 4, which were observed in the 4.5 m long beam, were cushioned by both the development of the hinges at the two supports and the lower axial stiffness of the beam. The development of the catenary action between the point 5 and point 6 was then delayed. The increase in span length, the degradation of the elastic modulus and the increased second-order effects led to higher deformations at the mid-span, reducing the axial force developed between the point 6 and point 7. The observations suggest that the end-support conditions and the span length affect the fluctuations of the axial force response when the beam is exposed to the traveling fire. Similar conclusion was made in [11], i.e., the structural system affects the cyclic structural responses.

When the responses between the 4.5 m beam heated by the furnace fire and the 9 m beam heated by the TG1 curve are compared, Fig. 11 indicates that the studied beams are more sensitive to the gas temperatures than to the span length. The fire with a higher temperature and faster heating rate accelerated the occurrence of large deformation. In contrast, the TG1 fire developed slowly with multiple local peaks also producing a multiple plastic hinge mechanism, which delayed the activation of the catenary action.

4.3. Effect of heating locations on the response of 9 m long beam

The effect of heating locations on the beam response was studied by locally heating the 9 m long beam using TG2 curve. The beam was heated both in the middle of the span and close to supports as the plastic hinges were developed at these regions. These scenarios can also take place if the fire ignites and heats the beam locally. Fig. 17 and Fig. 18 respectively show the mid-span displacement and the axial force of the beam heated by these two scenarios. The scheme of heating the beam is

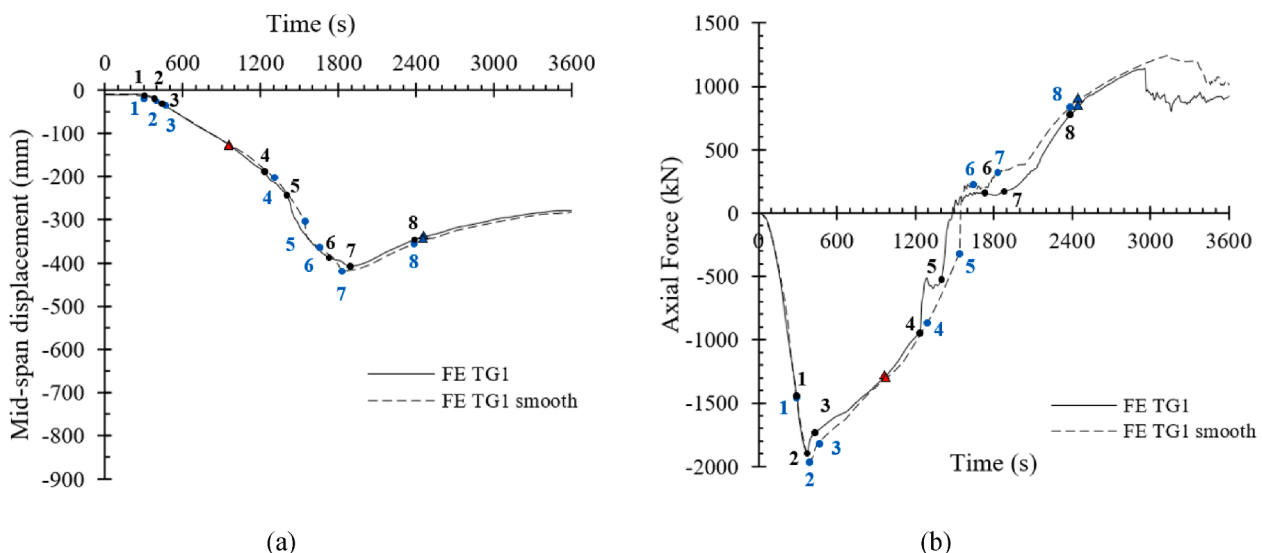


Fig. 15. Response of the 9 m long beam heated with the TG1 curve and the TG1 smooth curve: (a) Mid-span displacement (b) Axial force response at end-support.

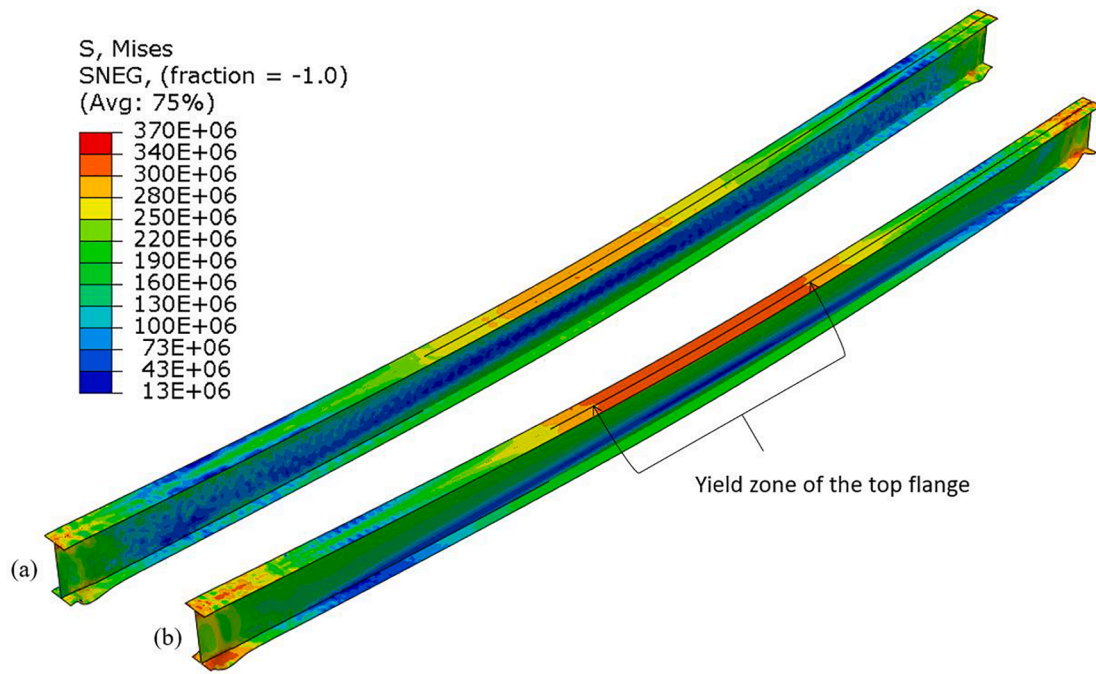


Fig. 16. Deformation mode at 1300 s of the 9 m steel beam heated by (a) TG1 curve and (b) TG1 smooth curve (units in N/m^2).

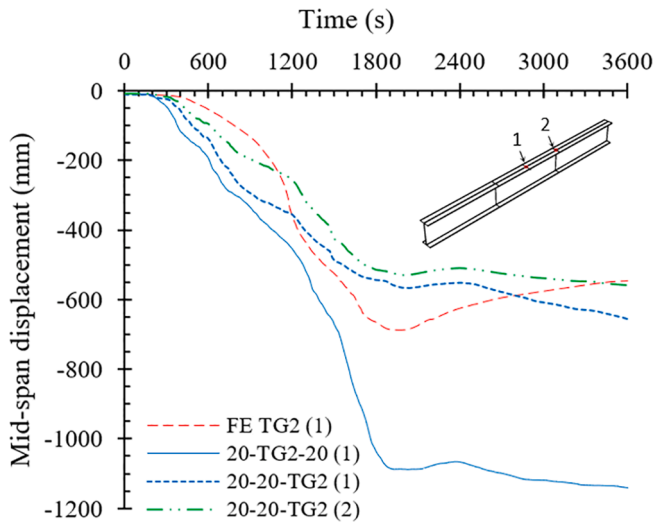


Fig. 17. Mid-span displacement of the 9 m long beam heated with TG2 curve locally and uniformly along the span.

mentioned in the figures as 20–20-TG2 and 20-TG2-20, where 20 represents 20 °C, TG2 represents the fire curve, and the location of TG2 in the symbol represents the heated segment in the studied beam. The numbers in the brackets, i.e., 1 or 2, represents the location of the displacement output.

The results in Fig. 17 and Fig. 18 show that, compared to the beam heated uniformly, the beam heated locally transformed more suddenly from a compression-controlled state to a bending-controlled state, thus leading to a much earlier transition of the axial force from compression to tension. In the beam heated in the middle, the sudden transitions were due to the locally degraded materials within highly stressed region (the mid-span) unable to hold the load. In contrast, heating the segment close to the support developed a lower compressive force as the longer colder segment had a lower axial stiffness. Since the local heating was away from the mid-span of the beam, the transition from compression to tension was delayed, and the beam also deflected less. The two locally

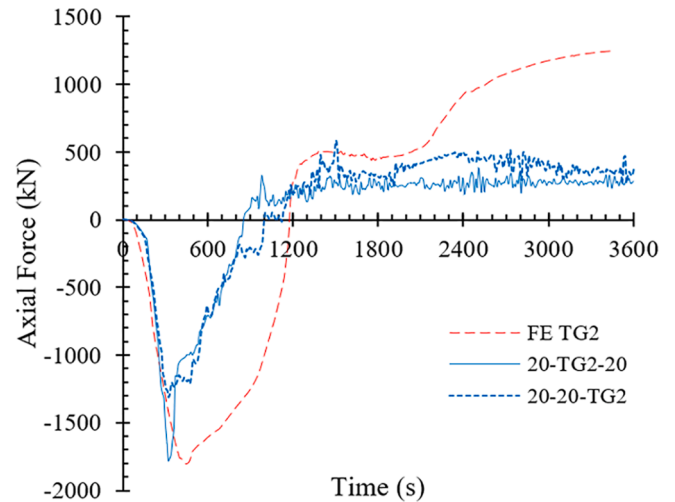


Fig. 18. Axial force response of the 9 m long beam heated with TG2 curve locally and uniformly along the span.

heated beams also activated the transition by the plastic hinge at mid-span, as the two beams deflected with a rate similar to the uniformly heated beam at around 1200 s. In addition, the difference in deflection curves between two locally heated beams was larger up to 1200 s and became smaller afterwards. The trend showed the transition from a bending-controlled behaviour to a tension-controlled behaviour.

The results indicate that local heating of the beam at highly stressed region (i.e., the mid-span) can be more detrimental, leading to early failure compared to uniform heating of the whole span of the beam. When a long beam attains high temperatures locally, the degraded material in the highly stressed region is unable to carry the load, therefore limiting the capacity of the beam. A similar phenomenon can occur inside the beam when it is heated non-uniformly by a travelling fire.

4.4. Effect of load ratios on the response of 9 m long beam

The effect of the load ratios on the response of the 9 m long beam heated by a travelling fire was studied using the load ratios of 0.3 and 0.5. Fig. 19(a) shows that the deflection of the beam was larger with the load ratio of 0.5 than with the load ratio of 0.3. The deflections of the beams started to deviate at 200 s after the degradation of the elastic modulus, and the differences were larger between 700 s and 1100 s. The beam with the load ratio of 0.5 ran away about 300 s earlier than the beam with the load ratio of 0.3.

As shown in Fig. 19(b), compared to the beam with the load ratio of 0.3, the beam with the load ratio of 0.5 had a lower peak of the compressive force and transitioned the axial force from compression to tension about 700 s earlier. The fluctuations of the axial forces can be explained by the stress contour developed inside the beam. At 360 s, the stress contour in Fig. 20(a) shows that the beam with the load ratio of 0.5 was highly stressed in the regions close to the supports and at the mid-span. The yield of the material reduced the stiffness of the beam in the highly stressed regions, thus lowering the peak value of the axial force. In addition, the load-carrying capacity of the beam was also limited by the local buckling of the flanges close to the supports. At 540 s when the TG1 curve reached the first peak, the additional highly stressed region in the web was also observed close to the mid-span as shown in Fig. 20(b). At 700 s when TG2 curve reached its peak value, the TG1 curve reached its second peak. The catenary action was activated before the degradation of effective yield strength at 400 °C. Fig. 20(c) showed that the previously yielded regions close to mid-span were unloaded to the elastic range. At 1100 s when the TG3 curve reached its peak, Fig. 20(d) shows that the beam yielded more at the mid-span region. At 1700 s, the plastic hinge formed inside this region triggered the final runaway failure of the beam. The loading and unloading from elastic range to plastic range accelerated the beam entering into catenary action.

The development of von Mises stress at the mid-span of the beams for the two load ratios are presented in Fig. 21. The points marked in the figure are correlated to the points marked in Fig. 19. The heating-cooling cycles of the travelling fire affected the axial force development in beam more clearly with the load ratio of 0.5 than with the load ratio of 0.3 before 700 s. At the load ratio of 0.5, the initial thermal bowing caused by non-uniform temperature field across the cross-section yielded more material in compression region. As shown in Fig. 21(a), the Von Mises stress output on the top flange of the beam at mid-span exceeded the yield strength at 200 s. Further increased temperature degraded the elastic modulus, thus initiating the unloading of

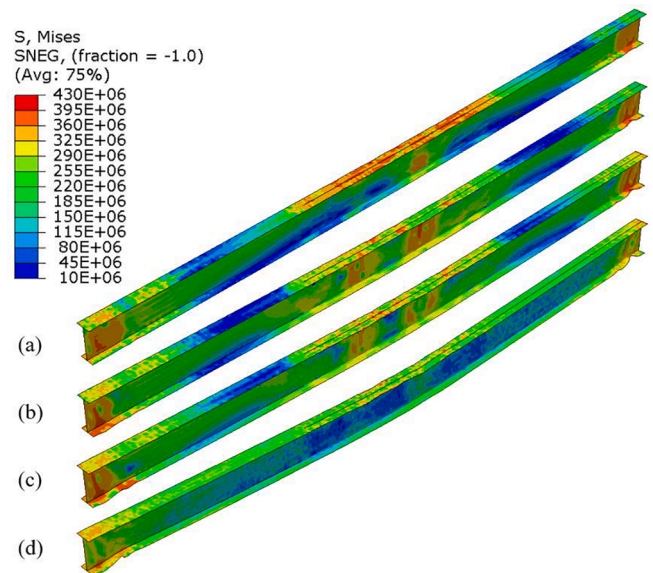


Fig. 20. Stress contour of the 9 m steel beam exposed to travelling fire with the load ratio of 0.5 at different times: (a) 360 s (point 2) (b) 540 s (point 4) (c) 700 s (point 5) (d) 1100 s.

the material in compression. As shown in Fig. 21(b), the von Mises stress of the upper part of the web (close to the top flange) was reduced. The unloading of the yielded parts of the beam led to the residual deformation of the beam. This deformation was further enlarged by the cyclic axial forces created by the non-uniform temperature field along the beam. When the catenary action inside the beam was activated at around 700 s, Fig. 21 shows that the beam in the mid-span was loaded either below or close to the yield strength. The fluctuations in von Mises stresses at early stages were not observed for the beam with load ratio of 0.3. At 1100 s, the beams with both load ratios had similar stresses as shown in Fig. 21 for both the top flange and the web, thus indicating similar mechanism inside the beams. This observation suggests that the fluctuations experienced by the beams with the load ratio of 0.5 result in yielding of the material at the mid-span of the beam in a cyclic manner. This cyclic yielding accumulates and contributes to accelerated deformation early on.

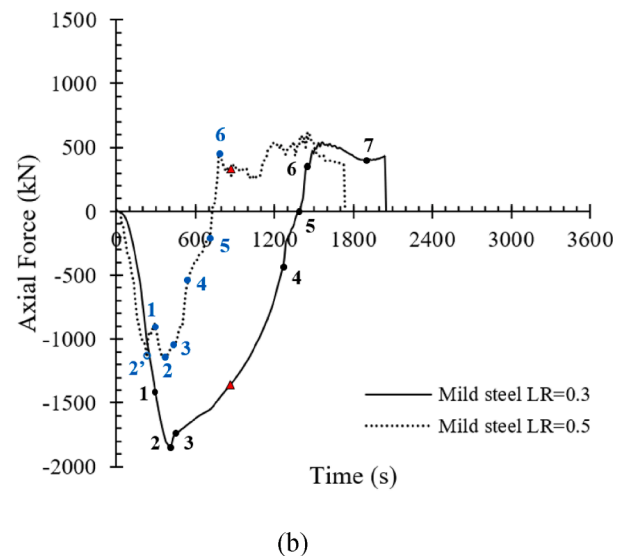
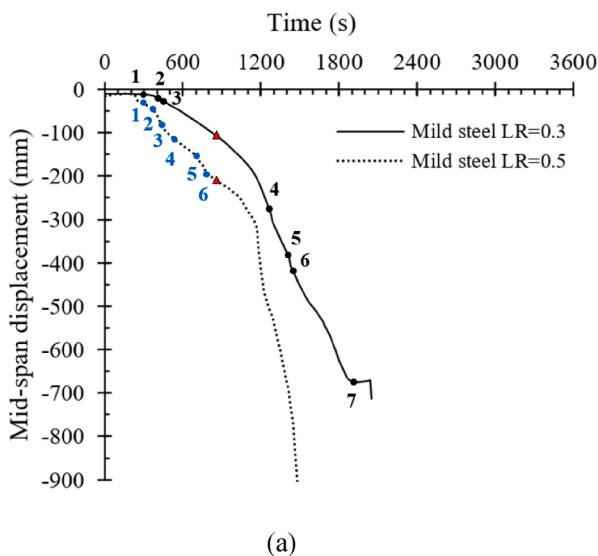


Fig. 19. Effect of load ratios on the response of the 9 m long beam: (a) Mid-span displacement (b) Axial force response at end-support.

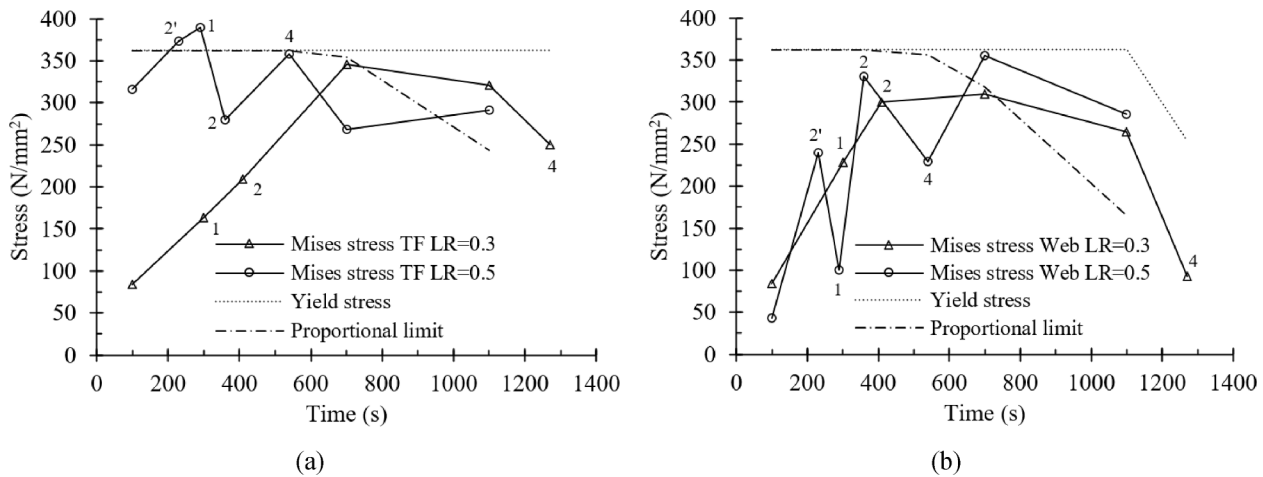


Fig. 21. Comparison of the von Mises stress development at the mid-span of the beams with load ratio of 0.3 and 0.5 in the (a) top flange (TF) and (b) upper part of the web. The numbers refer to the points in Fig. 19.

4.5. Effect of material strength on the response of 9 m long beam

The effects of the material strength on the response of the 9 m beams exposed to travelling fire were studied using mild steel and HSS. The effect of material strength was considered for the load ratios of 0.3 and 0.5.

The material modelling was based on EN 1993-1-2 [14]. In addition to the reduction factors given in EN 1993-1-2 for mild steel (S355) and HSS (S700) [14], similar reduction factors presented in [27] were also used. The stress–strain curves in [27] were measured from the tests up to 800 °C. As shown in Fig. 22, a clear disparity was observed in the curves from 200 °C to 700 °C between the test and the code values. The measured values are lower in strength but have a larger elastic modulus than the corresponding code values. The detailed differences in the reduction factors are compared in Fig. 23.

Fig. 24 and Fig. 25 show the mid-span displacement and the axial force response of the 9 m long beam with the load ratios of 0.3 and 0.5. The stages of the axial force response of HSS beam are marked on the curve in Fig. 24. For the load ratio of 0.3, the figure shows that the peak axial force in compression of the HSS beam was twice as large as the value for the mild steel beam. The higher compression force led to a

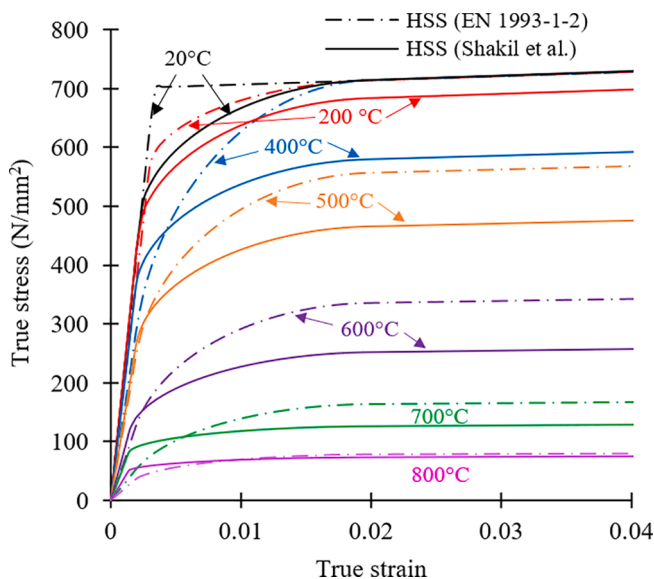


Fig. 22. Material model of HSS based on the equations in EN 1993-1-2 but with reduction factors both from the same design code [14] and from [27].

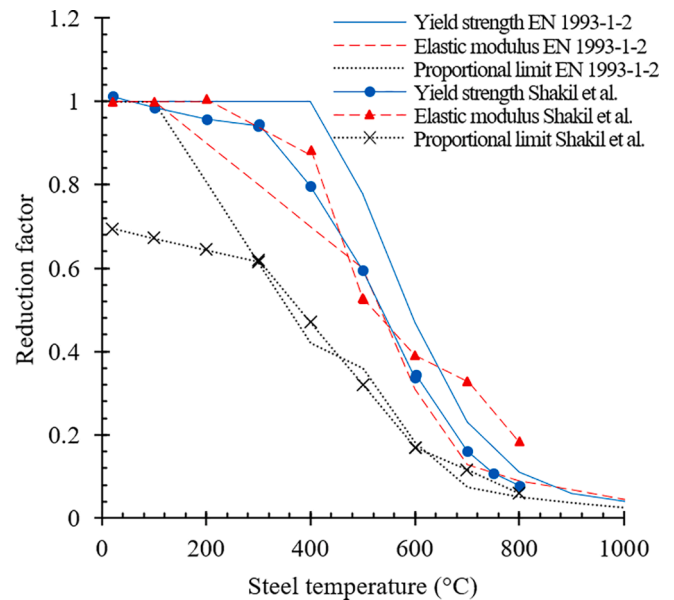


Fig. 23. Reduction factors in EN 1993-1-2 [14] and from the tests [27] for predicting the degradation of mechanical properties of HSS.

more sudden transition from a compression-controlled behaviour to a bending-controlled behaviour. The transition from compression to tension occurred about 200 s earlier in the HSS beam than the mild steel beam. In addition, the cyclic axial forces induced by the heating–cooling cycles of the fire curves were more observable in the HSS beam than the mild steel beam. Under the load ratio of 0.3, the HSS beams modelled by measured values and code values behaved similarly until Stage 7. After that, the beam modelled using the mechanical properties given in the code distorted largely and failed. The beam modelled using the measured mechanical properties survived by hanging on the supports.

In Fig. 25, both the mild steel and HSS beams with the load ratio of 0.5 had similar trends and values of the mid-span displacement. For all the beams, the catenary action was triggered before the degradation of effective yield strength at 400 °C. However, the transition occurred around 300 s earlier in the HSS beam using measured values than in both the mild steel and HSS beams using the code values. As the elastic range is larger for the HSS beam than for the mild steel beam, the travelling fire created a higher cyclic axial force in the HSS beam than in the mild steel beam. The HSS beam modelled using the measured values had more

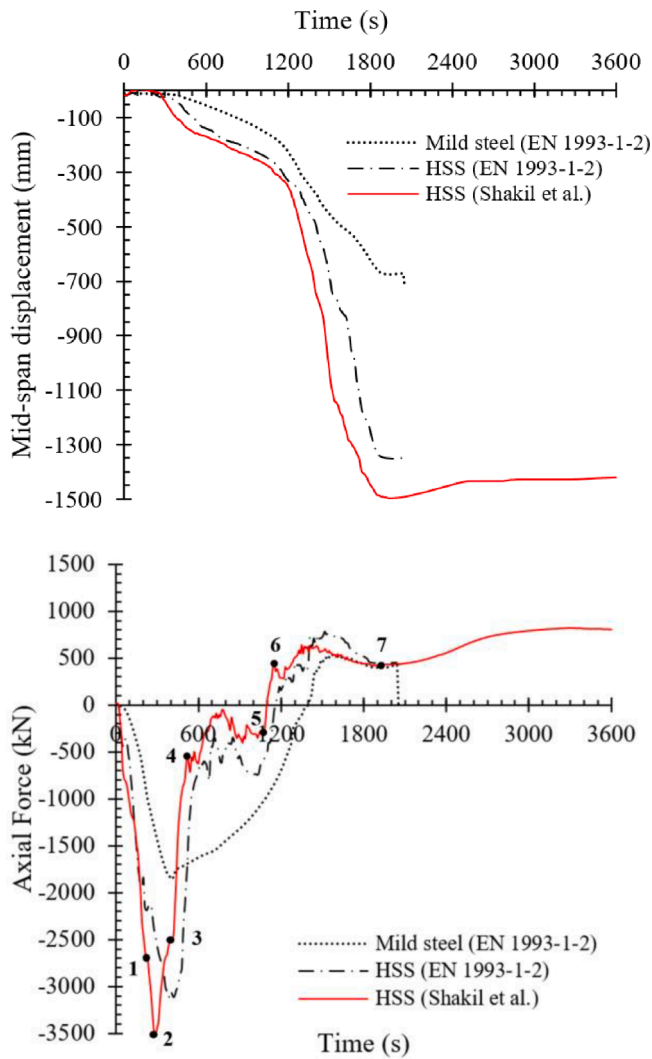


Fig. 24. FE results of the mid-span displacement and axial force response of the 9 m long beam with the load ratio of 0.3.

pronounced cyclic axial force response than the HSS beam modelled using the code values. In addition, all the beams experienced runaway deflection at the same time in a similar mechanism due to the highly degraded material properties close to the mid-span.

Compared to mild steels, the HSS material has longer elastic range, thus leading to the larger fluctuations in the axial force response of the beam. At lower load ratios, the HSS beams developed considerably higher compressive axial force than the mild steel beams. When the fluctuations and the magnitude of axial forces are large, their effect on the design of the connections at the supports should be considered, especially during the cooling stage. In this study, the effect of the cooling rate on the mechanical properties was not considered. Under the load ratio of 0.5, the heating–cooling cycles activated the catenary action before the degradation of the effective yield strength at elevated temperatures due to the accumulated residual deformations during the unloading of the yielded part of the beam. Compared to the HSS beam modelled using code values, the HSS beam modelled using the measured values activated the catenary action 300 s earlier and oscillated heavily due to larger degradation in strength and less degradation in elastic modulus. The larger deflections that activate the catenary action should be considered in the practical design. Therefore, the criteria to determine the critical temperatures of the beams exposed to the travelling fire are studied further.

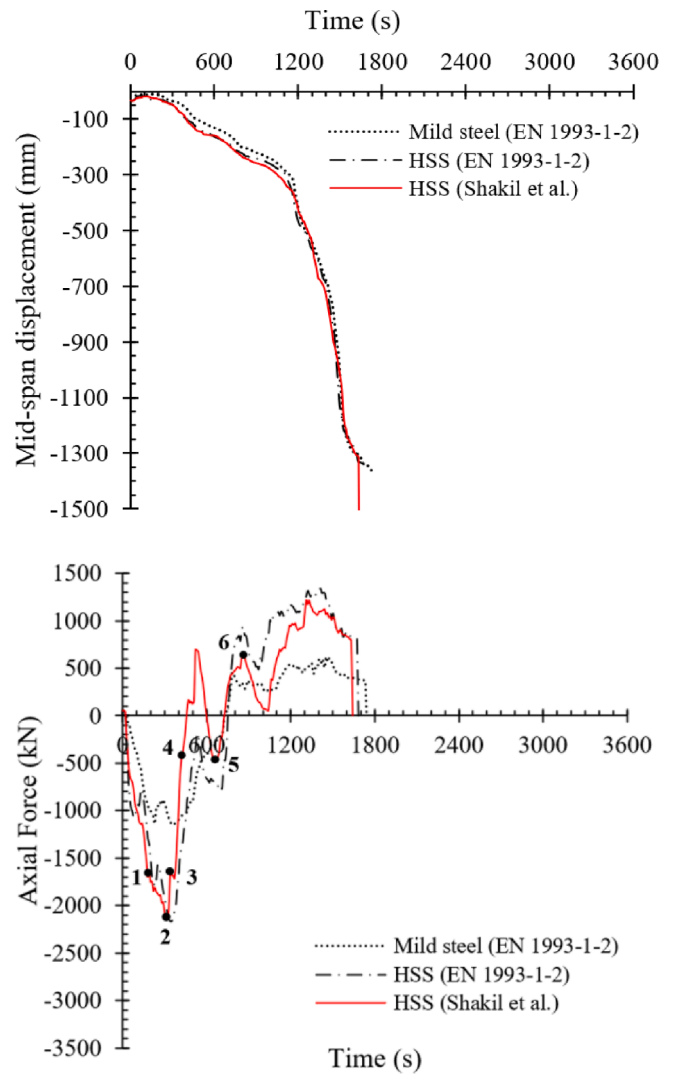


Fig. 25. FE results of the mid-span displacement and axial force response of the 9 m long beam with the load ratio of 0.5.

5. Critical temperatures of beams heated non-uniformly

5.1. Criteria for the determination of critical temperatures

The deflection limit and the deflection rate limit given in EN 1363-1 [18] were used to determine the critical temperatures of the beams exposed to the travelling fire as in the previous studies on the responses of the unprotected steel beams heated uniformly in [33]. According to EN 1363-1, the deflection limit is defined as.

$$D_{limit} = \frac{L^2}{400d} [mm] \tag{1}$$

and the deflection rate limit is defined as

$$\left(\frac{dD}{dt}\right)_{limit} = \frac{L^2}{9000d} [mm/min] \tag{2}$$

where L is the span, and d is the distance between the extreme fibre of compression and tension zone of the beam section. The structure fails when either deflection exceeds $1.5 \times D_{limit}$, or both D_{limit} and $(dD/dt)_{limit}$ are exceeded. The critical temperature of the beam is the temperature taken at the time when either of the criteria is fulfilled first. In this study, the times at limiting deflection t_{DL} and deflection rate t_{DR} were used for defining the temperatures θ_{DL} and θ_{DR} , respectively. Temperatures

$\theta_{1.5 \times DL}$ corresponding to the time at $1.5 \times D_{limit}$ were also determined.

As shown in their load-bearing mechanisms, all the studied beams developed catenary actions. Some of the studied beams hung from the supports until the start of cooling, while others had runaway deflections because the degraded material was unable to carry the mechanical loads at elevated temperatures. Therefore, the temperature θ_{cat} at which the catenary action was developed was also determined and compared to the critical temperatures received using EN 1363-1 criteria. This temperature can be further used to determine the formation of axial tension forces inside the beams.

As a simplification, the critical temperatures can also be determined according to the strength criterion i.e., the temperatures at which the load ratio of the beam corresponds to the reduction factors of yield strength. Similar methods have been used in the studies for cold-formed steel wall stud in [37]. Therefore, critical temperatures $\theta_{cr,LR,EC3}$ based on the reduction factors given in EN 1993-1-2 [14] and critical temperatures $\theta_{cr,LR,Shakil}$ based on the measured reduction factors for HSS in [27] were also determined for the studied beams.

5.2. Critical temperatures determined using different criteria

All the critical temperatures determined for the studied beams are presented in Table 2. In the table, the studied beams are classified by length as long or short, steel grade as mild steel, HSS, or HSS-Shakil, and fire scenarios as Furnace, TG1, TG2, TG3 or All. For instance, ‘short-mild-furnace’ means the 4.5 m long beam made of mild steel and heated by furnace fire.

For the steel beams with the studied boundary conditions and mechanical loads in this research, the critical temperatures of the beams were determined according to the temperatures of the bottom flange at the mid-span because the hinge mechanism was activated there. The temperature of the bottom flange at the mid-span corresponding to the time at which the limit criteria was satisfied was taken as the critical temperature. In Table 2, the critical temperatures and the corresponding times according to EN 1363-1 criteria are underlined. For the case of long-mild-TG1, the critical temperature according to EN 1363-1 criteria was not reached. For the cases of long-mild-TG2 and long-mild-all, the deflection limit of $1.5 \times D_{limit}$ was reached in the cooling stage.

5.3. Comparison of critical temperatures determined using different criteria

Critical temperatures determined according to EN 1363-1 and the temperatures corresponding to catenary actions are presented in Fig. 26 (a) and (b), respectively, and compared with the reduction factors for both proportional limit and effective yield strength given in EN 1993-1-2

[14]. The reduction factors for effective yield strength measured for HSS in [27] are also added in Fig. 26.

For the beams with the load ratio of 0.3, Fig. 26(a) shows that the critical temperature according to EN 1363-1 determined for ‘short-mild-furnace’ was lower than those corresponding to the reduction factors for the effective yield strength given in EN 1993-1-2 and in [27]. The observed differences were due to the average temperature used for determining the critical temperatures and the maximum temperature used for determining the reduction factors in the code. For the rest of the beams heated both uniformly and non-uniformly, the critical temperatures according to EN 1363-1 were equal to or higher than those corresponding to the reduction factors for the effective yield strength. For the beams with the load ratio of 0.3, the catenary action temperatures as presented in Fig. 26(b) were slightly higher than the critical temperatures corresponding to the reduction factors for the effective yield strength, which agreed well with the mechanism of catenary action due to large deformations.

For the load ratio of 0.5, Fig. 26(a) shows that the critical temperatures determined according to EN 1363-1 criteria were slightly higher than those corresponding to the reduction factors in EN 1993-1-2. The temperatures at catenary action in Fig. 26(b) were approximately 330 °C lower than EN 1363-1 critical temperatures, and 180 °C lower than the critical temperatures according to the yield strength reduction factors. The temperatures at catenary actions for the studied beams with load ratio of 0.5 were close to those corresponding to the reduction factors of proportional limit in EN 1993-1-2. Since the runaway deflection for the beams with load ratio of 0.5 occurred after the development of catenary action, the temperatures determined at runaway are presented in parentheses in Table 2.

Table 2 and Fig. 26 indicate that the beams with lower load ratio can be designed using the reduction factors in EN 1993-1-2 and [27], but complemented by the critical temperatures determined using the EN 1363-1 criteria. Since the transfer of bending-controlled behaviour to axial-stress controlled behaviour threatens the beam integrity, the catenary action temperatures should be considered for the design of the beams with the load ratio of 0.5. When temperatures at catenary actions are considered as critical temperatures for the beams, they agree well with the critical temperatures according to EN 1363-1 at the load ratio of 0.3. However, for the load ratio of 0.5, the temperatures at catenary actions were significantly lower than EN 1363-1 critical temperatures and the critical temperatures according to the yield strength reduction factors. These observations suggest that early activated catenary action can delay the runaway failure when the end-connections are designed to withstand the induced axial forces. However, for the integrity of the beam structures, the yield strength based on the proportional limit is recommended for the design of beams (according to EN 1993-1-2) at

Table 2
Critical temperatures for the beams exposed to uniform and non-uniform fires.

Studied beams	Load ratio	Runaway	^a Temperatures from FE results (°C)				Time at temperatures from FE results (s)				Critical temperatures based on reduction factors (°C)	
			$\theta_{1.5 \times DL}$	θ_{DL}	θ_{DR}	θ_{cat}	$t_{1.5 \times DL}$	t_{DL}	t_{DR}	t_{cat}	$\theta_{cr,LR,EC3}$	$\theta_{cr,LR,Shakil}$
			short-mild-furnace	0.3	no	720	<u>580</u>	500	750	880	<u>720</u>	660
short-mild-TG1	0.3	no	<u>670</u>	500	680	650	<u>1610</u>	1160	1680	1520	670	625
long-mild-TG1	0.3	no	–	–	600	680	–	–	1440	1700	670	625
long-mild-TG2	0.3	no	775 (cooling stage)	<u>745</u>	475	780	1840	1315	960	1400	670	625
long-mild-TG3	0.3	yes	945	<u>780</u>	515	880	1760	1580	1320	1650	670	625
long-mild-all	0.3	yes	760 (cooling stage)	<u>810</u>	640	800	1900	<u>1500</u>	1140	1450	670	625
long-mild-all	0.5	yes	780	<u>690</u>	590	350* (800**)	1400	<u>1210</u>	1080	800 (1450**)	590	540
long-HSS-all	0.3	yes	810	<u>760</u>	640	700	1500	<u>1350</u>	1140	1200	670	625
long-HSS-all	0.5	no	805	<u>700</u>	640	385* (780**)	1390	<u>1200</u>	1140	850 (1400**)	590	540
long-HSS Shakil-all	0.3	yes	770	<u>730</u>	590	645	1380	<u>1270</u>	1080	1150	670	625
long-HSS Shakil-all	0.5	yes	750	<u>720</u>	590	385* (740**)	1340	1225	1080	850 (1300**)	590	540

^aCritical temperatures according to EN 1363-1 are underlined.

*Catenary action triggered before 400 °C.

**Temperature and time when actual plastic hinges were formed.

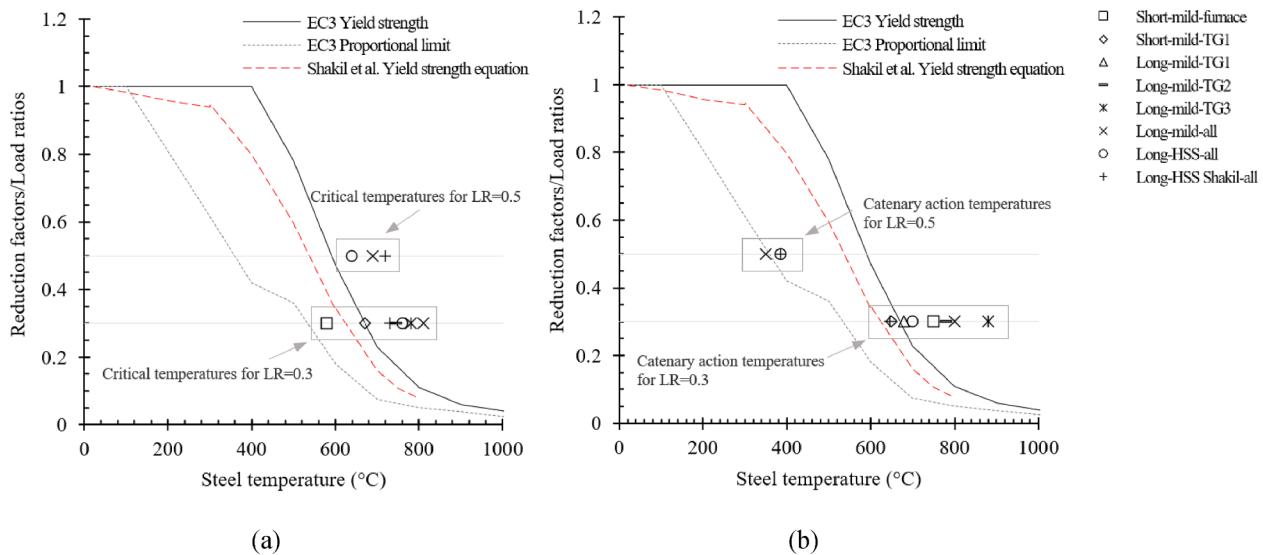


Fig. 26. Comparison of critical temperatures determined for different load ratios (LR) using reduction factors given in EN 1993-1-2 and in [27] with (a) critical temperatures according to EN 1363-1 limiting criteria and (b) temperatures at catenary action.

high load ratios exposed to the travelling fire. For further simplification, a critical temperature of 350 °C as proposed for the structural fire design of cold-formed steel members in [14] can also be considered.

In this study, the critical temperatures were determined at the bottom flange of the cross-section at mid-span. For the beams with highly non-uniform temperature field both across the cross-section and along the span, the critical temperatures can be determined according to either the maximum temperature or the average temperatures reached at the critical section of the beam. The failure of the steel beams can be defined in the time domain when using the advanced analyses. The applicability and the accuracy of the criteria for the practical use need further research.

6. Conclusions

A five-stage mechanism was developed to characterize the load-bearing behaviour of the beams exposed to different fire scenarios. The mechanism was used for studying the sensitivity of the beam response to fire exposure, span length, load ratio and strength grade of steel. The critical temperatures based on the deflection and strength criteria, and the temperatures at the time of the development of catenary action were determined for the beams exposed to travelling fires. The following specific conclusions are drawn from the studies:

- For the beams exposed to the travelling fire, the beams within elastic range are prone to the fluctuations of the axial force. These fluctuations are mainly caused by non-uniform temperature field along the beam exposed to gas temperatures with multiple peaks.
- At higher load ratio, plastifications of the material cushioned the fluctuations in the axial force response. However, if the beams are unloaded from plastic range to elastic range during the heating-cooling cycles, the accumulation of the residual deformations can lead to the activation of catenary actions at temperatures below 400 °C.
- For the critical temperatures of the beams of both mild steel and HSS exposed to travelling fire, the values determined using the deflection limit and the deflection rate criteria given in EN 1363-1 agreed well with those determined by the strength criteria. For the beams with a higher load ratio, the temperatures activating catenary actions can be critical and should also be considered for the beam design. Alternatively, the beams can be designed according to the strength

criteria by using the effective yield strength based on the proportional limit.

- The HSS beams exposed to the travelling fire at lower load ratio develop higher axial compression forces compared to the mild steel beams and had more fluctuating axial force response due to the prolonged elastic range. Both higher value and fluctuation of axial force can be detrimental for the connections.
- Local heating of the beam at critical regions can be more detrimental than uniform heating of the entire beam due to the local degradation of materials within a highly stressed region indicating that the start of travelling fire with a large heat release rate close to highly stressed region should be considered in the design.

The understanding of the behaviour of single span beams exposed to a travelling fire developed through the current work can be used for future research involving complex travelling fire scenarios and structural configurations. This understanding can further be extended to study the effect of rapid cooling due to fire-fighting intervention on the structural response.

Declaration of Competing Interest

The authors declare that they have no known competing financial interests or personal relationships that could have appeared to influence the work reported in this paper.

Acknowledgements

The authors acknowledge the Academy of Finland for supporting the current research (Project no. 289037) and the Foundation for Aalto University Science and Technology, Finland.

References

- [1] Zhang C, Li G-Q. Fire dynamic simulation on thermal actions in localized fires in large enclosure. *Adv Steel Constr* 2012;8(2):124–36.
- [2] Stern-Gottfried J, Rein G. Travelling fires for structural design—Part I: Literature review. *Fire Saf J* 2012;54:74–85.
- [3] Spinardi G, Bisby L, Torero J. A review of sociological issues in fire safety regulation. *Fire Technol* 2017;53(3):1011–37.
- [4] Wang YC, Burgess I, Wald F, Gillie M. Performance-based fire engineering of structures. CRC Press; 2012.
- [5] Dai X, Jiang L, Maclean J, Welch S, Usmani A. Implementation of a New Design Travelling Fire Model for Global Structural Analysis. In: *Proceedings of the 9th International Conference on Structures in Fire*; 2016. p. 959–66.

- [6] Dai X, Welch S, Usmani A. A critical review of “travelling fire” scenarios for performance-based structural engineering. *Fire Saf J* 2017;91:568–78.
- [7] Alam N, Nadjai A, Charlier M, Vassart O, Welch S, Sjöström J, et al. Large scale travelling fire tests with open ventilation conditions and their effect on the surrounding steel structure – The scnd fire test. *J Constr Steel Res* 2022;188:107032.
- [8] Clifton CG. “Fire Models for Large Firecells,” HERA Report R4-83, 1996.
- [9] Stern-Gottfried J, Rein G. Travelling fires for structural design-Part I: Literature review. *Fire Saf J* 2012;54:74–85.
- [10] Stern-Gottfried J, Rein G. Travelling fires for structural design-Part II: Design. *Fire Saf J* 2012;54:96–112.
- [11] Rackauskaite E, Kotsovinos P, Rein G. Structural response of a steel-frame building to horizontal and vertical travelling fires in multiple floors. *Fire Saf J* 2017;91:542–52.
- [12] Rackauskaite E, Kotsovinos P, Jeffers A, Rein G. Structural analysis of multi-storey steel frames exposed to travelling fires and traditional design fires. *Eng Struct* 2017;150:271–87.
- [13] Ramsamy VR, Annerel E, Van Maele K, Maragkos G, Merci B. “Analysis of Travelling Fire and Comparison to the Travelling Fire Methodology,” *SFPE Europe*, <https://www.sfpe.org/publications/sfpeeuropedigital/sfpeurope20/europeissue20feature3>, no. 20, 2020.
- [14] EN 1993-1-2, “Design of steel structures - Part 1-2: General rules - Structural fire design,” CEN, Brussels, 2005.
- [15] Liu T. Effect of connection flexibility on fire resistance of steel beams. *J Constr Steel Res* 1998;45(1):99–118.
- [16] Li G-Q, Guo S-X. Experiment on restrained steel beams subjected to heating and cooling. *J Constr Steel Res* 2008;64(3):268–74.
- [17] Liu T, Fahad MK, Davies JM. Experimental investigation of behaviour of axially restrained steel beams in fire. *J Constr Steel Res* 2002;58(9):1211–30.
- [18] EN 1363-1:2020, “Fire resistance tests - Part 1: General requirements,” CEN, Brussels, 2020.
- [19] British Standard Institution, “Fire Tests on Building Materials and Structures. Part 20. Method of determination of fire resistance of elements of constructions,” BS 476, 1987.
- [20] Dwaikat MM, Kodur VK. A performance based methodology for fire design of restrained steel beams. *J Constr Steel Res* 2011;67(3):510–24.
- [21] Yin Y, Wang Y. A numerical study of large deflection behaviour of restrained steel beams at elevated temperatures. *J Constr Steel Res* 2004;60:1029–47.
- [22] Guo Z, Huang S-S. Behaviour of restrained steel beam with reduced beam section exposed to fire. *J Constr Steel Res* 2016;122:434–44.
- [23] Shakil S, Lu W, Puttonen J. “Simulation of the effect of non-uniform temperatures on a beam of high strength steel within a fire compartment,” in *9th International Conference on Steel and Aluminium Structures (ICSAS19)*, Bradford, UK, 2019.
- [24] Dwaikat M, Kodur V. Effect of location of restraint on fire response of steel beams. *Fire Technol* 2010;46(1):109–28.
- [25] Zhang C, Li G-Q, Usmani A. Simulating the behavior of restrained steel beams to flame impingement from localised fire. *J Constr Steel Res* 2013;83:156–65.
- [26] Zhang C, Gross JL, McAllister TP. Lateral torsional buckling of steel W-beams subjected to localized fires. *J Constr Steel Res* 2013;88:330–8.
- [27] Shakil S, Lu W, Puttonen J. Experimental studies on mechanical properties of S700 MC steel at elevated temperatures. *Fire Saf J* 2020;116:103157.
- [28] Dwaikat M, Kodur V. Engineering approach for predicting fire response of restrained steel beams. *J Eng Mech* 2011;137(7):447–61.
- [29] Abaqus 6.13 Analysis user guide, Providence, RI, USA: Dassault Systèmes, 2013.
- [30] Pacor Inc., “Pacor,” [Online]. Available: <https://www.pacorinc.com/>. [Accessed 7 December 2018].
- [31] EN 1991-1-2, “Actions on structures- Part 1-2: General actions - Actions on structures exposed to fire,” CEN, Brussels, 2002.
- [32] Wang Y, Wu J, Huang Z, Jiang J, Yuan G, Zhang Y, et al. Experimental studies on continuous reinforced concrete slabs under single and multi-compartment fires with cooling phase. *Fire Saf J* 2020;111:102915.
- [33] Shakil S, Lu W, Puttonen J. Response of high-strength steel beam and single-storey frame in fire: Numerical simulation. *J Constr Steel Res* 2018;148:551–61.
- [34] Horová K, Jána T, Wald F. Temperature heterogeneity during travelling fire on experimental building. *Adv Eng Softw* 2013;62(63):119–30.
- [35] McGrattan KB, McDermott RJ, Weinschenk CG, Forney GP. *Fire Dynamics Simulator, Technical Reference Guide, Sixth Edition, Special Publication (NIST SP)*, 2013.
- [36] Pournaghshband A, Afshan S, Theofanous M. Elevated temperature performance of restrained stainless steel beams. *Structures* 2019;22:278–90.
- [37] The steel Construction Institute, “Building Design Using Cold-formed Steel Sections: Fire Protection,” SCI Publication P129, 1993.